



Initial PD model test results

D2.5

Grant Agreement No.	883553
Start date of Project	01-04-2020
Duration of the Project	48 months
Deliverable Number	D2.5
Deliverable Leader	Chalmers
Dissemination Level	Public
Version	V2.0
Submission Date	05-07-2023
Authors	Håkan Nilsson, Chalmers Valery Chernoray, Chalmers



The opinions expressed in this document reflect only the author's view and in no way reflect the European Commission's opinions. The European Commission is not responsible for any use that may be made of the information it contains.

This project has received funding from the European Union's Horizon 2020 research and innovation programme under grant agreement No 883553.

Version #	Description	Author	Organisation	Date
0.1	First version based on material provided by: Petter Miltén, Valery Chernoray and Mikhail Tokarev	Håkan Nilsson	Chalmers	15-02-2022
0.2	2 nd draft including CAD images, measurement details and operating conditions	Håkan Nilsson and Valery Chernoray	Chalmers	19-02-2022
1.0	First final version	Håkan Nilsson and Valery Chernoray	Chalmers	21-02-2022
1.1	Added comprehensive overview of results, more details regarding experimental setup, and some discussions of the results.	Håkan Nilsson and Valery Chernoray	Chalmers	06-04-2023
2.0	Second final version	Håkan Nilsson and Valery Chernoray	Chalmers	30-06-2023

Release Approval

Name	Role	Date
Håkan Nilsson	WP Leader	30-06-2023
Jeremy Bricker	Technical Project Coordinator (TU Delft)	30-06-2023
Roelof Moll	Project Coordinator (TU Delft)	30-06-2023

History of Changes

- Version 1.0, submitted 24-03-2022, rejected March 2023.
- Version 2.0, submitted 05-07-2023.

Table of Contents

Executive Summary	5
1. Introduction	6
2. Geometry and experimental set-up	7
3. PIV results	13
4. Conclusions	19
Appendix A: Lobe geometry	23
Appendix B: Contour plots of phase-averaged U and V velocity components	24
Appendix C: Contour plots of phase-averaged W velocity component at the outlet	34
Appendix D: Examples of contour plots of standard deviation	38

List of figures

Figure 1: CAD geometry. Dimensions in meters.	8
Figure 2: Sketch of rig components. Blue arrows show flow direction, same in both modes. PIV cameras set up for "Outlet" measurement.	8
Figure 3: Photos of rig components.	9
Figure 4 : Inlet (left) and outlet (right) diffusers, and static pressure measurement hoses.	10
Figure 5: Two-camera stereo PIV set-up.	10
Figure 6: Example of particle image. It should be noted that the measurement plane is located at mid-height of the lobes, and that perspective makes it look like the upper lobe extends outside the channel. PIV can only measure what is visible, so the lobes also cover some of the flow. This effect can be seen in all the results. The upper lobe rotates clockwise and the lower lobe rotates counter-clockwise.	11
Figure 7: Descriptions of measurement regions and phase angles (cf. Figure 6). Regions are marked green. Top row: Full view. Center row: Inlet. Bottom row: Outlet. Left column: "0" degrees. Center column: "15" degrees. Right column: "30" degrees. See definitions of phase angles in Table 2.	14
Figure 8: Full view, examples of instantaneous velocity components at "0" degrees. Left: U-velocity. Right: V-velocity. Top: Pump 45 RPM. Center: Pump 55 RPM. Bottom: Turbine 45 RPM.	16
Figure 9: Full view, phase-averaged velocity components at "0" degrees. Left: U-velocity. Right: V-velocity. Top: Pump 45 RPM. Center: Pump 55 RPM. Bottom: Turbine 45 RPM.	18
Figure 10: Sequence combination at outlet, using data from outlet view (left) and zoomed full View (right), turbine 45 RPM, Phase-averaged U-velocity. Follow sequence from top to bottom of left column first and then second column. Angle change is 15 degrees.	20
Figure 11: Sequence combination at outlet, using data from outlet view (left) and zoomed full View (right), turbine 45 RPM, Phase-averaged V-velocity. Follow sequence from top to bottom of left column first and then second column. Angle change is 15 degrees.	21

Figure 12: Sequence combination at outlet, using data from outlet view (left) and zoomed full View (right), turbine 45 RPM, velocity vectors. Follow sequence from top to bottom of left column first and then second column. Angle change is 15 degrees. Vectors are approximately similarly scaled...	22
Figure 13: Full view, pump 45 RPM, phase-averaged velocity components. Left: U-velocity. Right: V-velocity. Top: "0" degrees. Center: "15" degrees. Bottom: "30" degrees.....	25
Figure 14: Full view, pump 55 RPM, phase-averaged velocity components. Left: U-velocity. Right: V-velocity. Top: "0" degrees. Center: "15" degrees. Bottom: "30" degrees.....	26
Figure 15: Full view, turbine 45 RPM, phase-averaged velocity components. Left: U-velocity. Right: V-velocity. Top: "0" degrees. Center: "15" degrees. Bottom: "30" degrees.....	27
Figure 16: Inlet view, pump 45 RPM, Phase-averaged velocity components. Left: U-velocity. Right: V-velocity. Top: "0" degrees. Center: "15" degrees. Bottom: "30" degrees.....	28
Figure 17: Inlet view, pump 55 RPM, Phase-averaged velocity components. Left: U-velocity. Right: V-velocity. Top: "0" degrees. Center: "15" degrees. Bottom: "30" degrees.....	29
Figure 18: Inlet view, turbine 45 RPM, Phase-averaged velocity components. Left: U-velocity. Right: V-velocity. Top: "0" degrees. Center: "15" degrees. Bottom: "30" degrees.	30
Figure 19: Outlet view, pump 45 RPM, Phase-averaged velocity components. Left: U-velocity. Right: V-velocity. Top: "0" degrees. Center: "15" degrees. Bottom: "30" degrees.	31
Figure 20: Outlet view, pump 55 RPM, Phase-averaged velocity components. Left: U-velocity. Right: V-velocity. Top: "0" degrees. Center: "15" degrees. Bottom: "30" degrees.	32
Figure 21: Outlet view, turbine 45 RPM, Phase-averaged velocity components. Left: U-velocity. Right: V-velocity. Top: "0" degrees. Center: "15" degrees. Bottom: "30" degrees.	33
Figure 22: Outlet view, pump 45 RPM, Phase-averaged W-velocity component (uncertain). Top: "0" degrees. Center: "15" degrees. Bottom: "30" degrees.	35
Figure 23: Outlet view, pump 55 RPM, Phase-averaged W-velocity component (uncertain). Top: "0" degrees. Center: "15" degrees. Bottom: "30" degrees.	36
Figure 24: Outlet view, turbine 45 RPM, Phase-averaged W-velocity component (uncertain). Top: "0" degrees. Center: "15" degrees. Bottom: "30" degrees.	37
Figure 25: Full view, examples of standard deviation at "0" degrees. Left: U-velocity. Right: V-velocity. Top: Pump 45 RPM. Center: Pump 55 RPM. Bottom: Turbine 45 RPM.	39

List of tables

Table 1: Global details of investigated cases	11
Table 2: Summary of PIV results, as in file folder. Phase angles in quotation marks are with respect to the first phase angle of that region. Phase angles in brackets are actual angles.	13

Executive Summary

This report relates to a part of Task 2.3 of the ALPHEUS project. The full description of Task 2.3 is supplied in the box below, for convenience, showing that the purpose of the PIV measurements of the present work (sub-tasks 2.3.2 and 2.3.3) is to validate CFD after some initial CFD studies and before the validated CFD methodologies are used for the further studies. The CFD validation and CFD results are reported in D2.4 and are not part of the present report.

Task 2.3: Multidisciplinary optimization of Positive Displacement RPT [M1-M24]

Task Leader: NTNU; Partners involved: Chalmers, NTNU

An initial design is available, and CFD will be performed on this design (2.3.1). An experimental test will be set up (2.3.2) and measurements will be performed at Chalmers using index matching PIV technique (2.3.3). Data from these tests will be used as a base for validation of the CFD results (2.3.4). A simplified FSI analysis and system dynamics investigation will be made, finding loads on the structure as well as possible problems due to cyclic pressure excitations leading to wave interference issues and seiche phenomena (2.3.5). All aspects taken into consideration, a multidisciplinary upscaling and optimization is carried out (2.3.6).

Although the PIV data itself is the most important deliverable, to be used in the best possible way during the CFD validation, the present report visualizes all the phase-averaged velocity components and gives examples of instantaneous velocity component distributions and their standard deviation. Further, some main features of the flow are discussed. All flow-images in the report can be reproduced by the postprocessing scripts that are supplied with the data, and the scripts can be adapted for the need of the CFD validation. The complete CAD files, experimental data, and post-processing scripts have been stored in the open access repository 4TU for the benefit of anyone who would like to use the results for CFD validation and further studies.

1. Introduction

The present work is a part of a task to design and study a positive-displacement reversible pump-turbine (see Figure 1). The specific purpose of the present work is to provide validation data for the CFD studies that form the main part of the task and are to be used for the main studies and design. Once validated, the comprehensive CFD results complement and extend the experimental results so the entire flow field of the machine can be investigated thoroughly. It should particularly be noted that the CFD studies are not part of the present deliverable, but part of deliverable D2.4. The present experimental part includes design, manufacturing and assembly of the rig, all the experimental activities, preparation and clean-up of data, post-processing and reporting.

The experimental measurements have been conducted using the PIV technique. This technique involves a laser sheet that illuminates particles in a plane of the flow. Using two consecutive high-resolution images of the particle positions it is possible to calculate the velocity of the particles. The particles are chosen so that they follow the flow without disturbing it, so the flow velocity is the same as the particle velocity. For each pair of high-resolution images, the result is a two-dimensional view of the instantaneous velocity distribution in the plane that the laser sheet illuminates. The laser sheet should be as thin as possible to maintain a clear definition of the plane that is intended to be measured. To be able to calculate the velocity of a particle, the same particle must be illuminated in both the images. Since the laser sheet should be very thin, and the camera is viewing the illuminated plane normal to that plane, it is therefore most common to measure the two velocity components that are tangential to the plane. That is also the case in the present work. However, for one of the measured regions a stereo PIV methodology has been applied, using two cameras. This methodology is capable of also calculating the velocity normal to the plane, for particles that are indeed illuminated in both images and that have moved in all three directions. This third component is more difficult to measure, and the results are more uncertain. Still, those results are reported as additional data for the CFD validation, if considered useful. The flow in the studied positive-displacement reversible pump-turbine is mostly two-dimensional, with velocity components in the studied PIV plane, so those velocity components are most significant.

The results that are presented are for the mid-height of the positive-displacement reversible pump-turbine. The initial measurements covered the entire extent of the machine (denoted “full view”). Those measurements were conducted for three case; two in pump mode, with two different rotational speeds, and one in turbine mode. The PIV measurements were triggered by the lobe position, such that the instantaneous velocity distribution was obtained 100 times for a particular lobe position. Taking the average of those 100 samples yields the phase-averaged velocity distribution, and calculating the standard deviation of those 100 samples yields a view of where the velocity components have greater variation from the average values. Once the initial measurements of the full view were completed, the entire procedure was repeated for more confined regions at the inlet and outlet of the machine. This allowed a greater resolution of the experimental data in those regions. As mentioned, for the outlet also the third velocity component was measured.

As mentioned, the purpose of the present deliverable is to provide the data to the group doing the CFD studies, for them to use for validation of their results. Still, this report shows images of all the phase-averaged results as well as examples of instantaneous velocity distributions and standard deviations. The results are also briefly discussed. The report, the data, the post-processing scripts and the CAD files, have been made available to the public through storage in the open access 4TU repository.

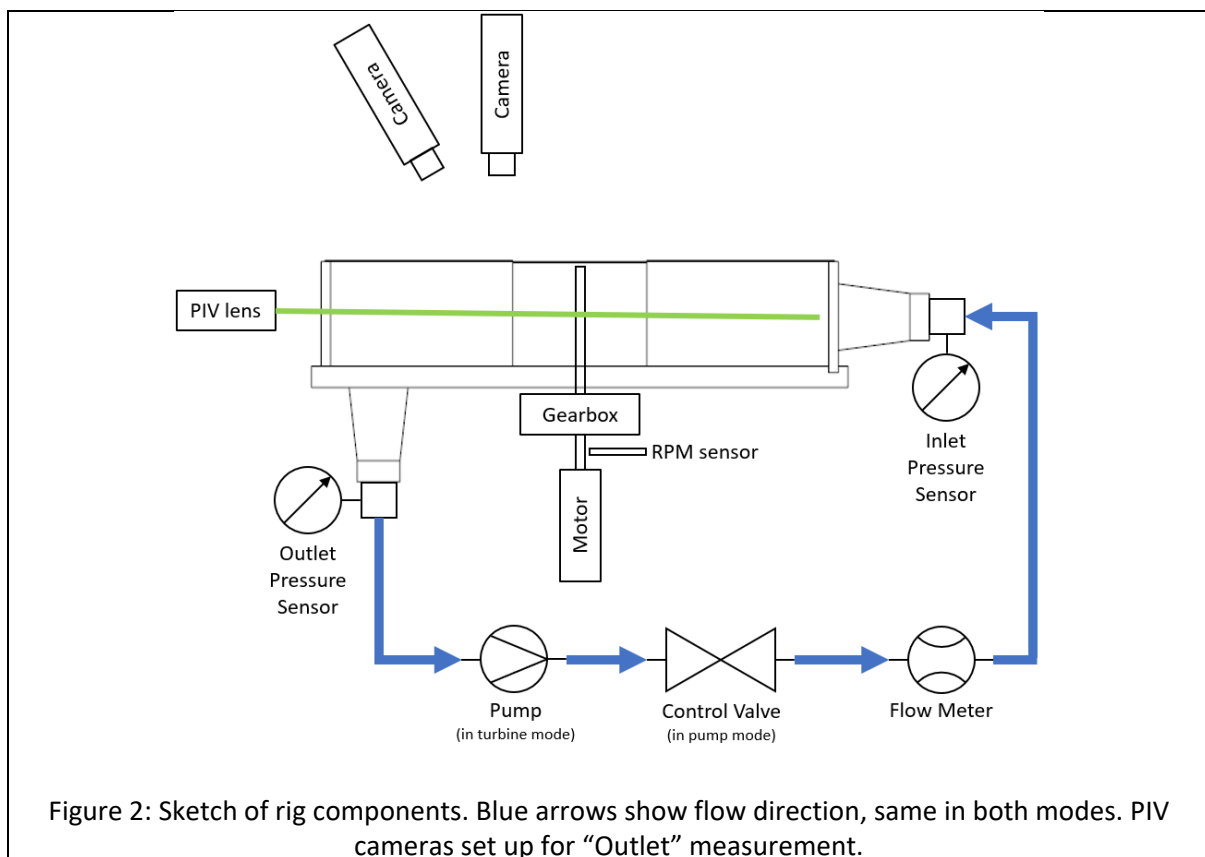
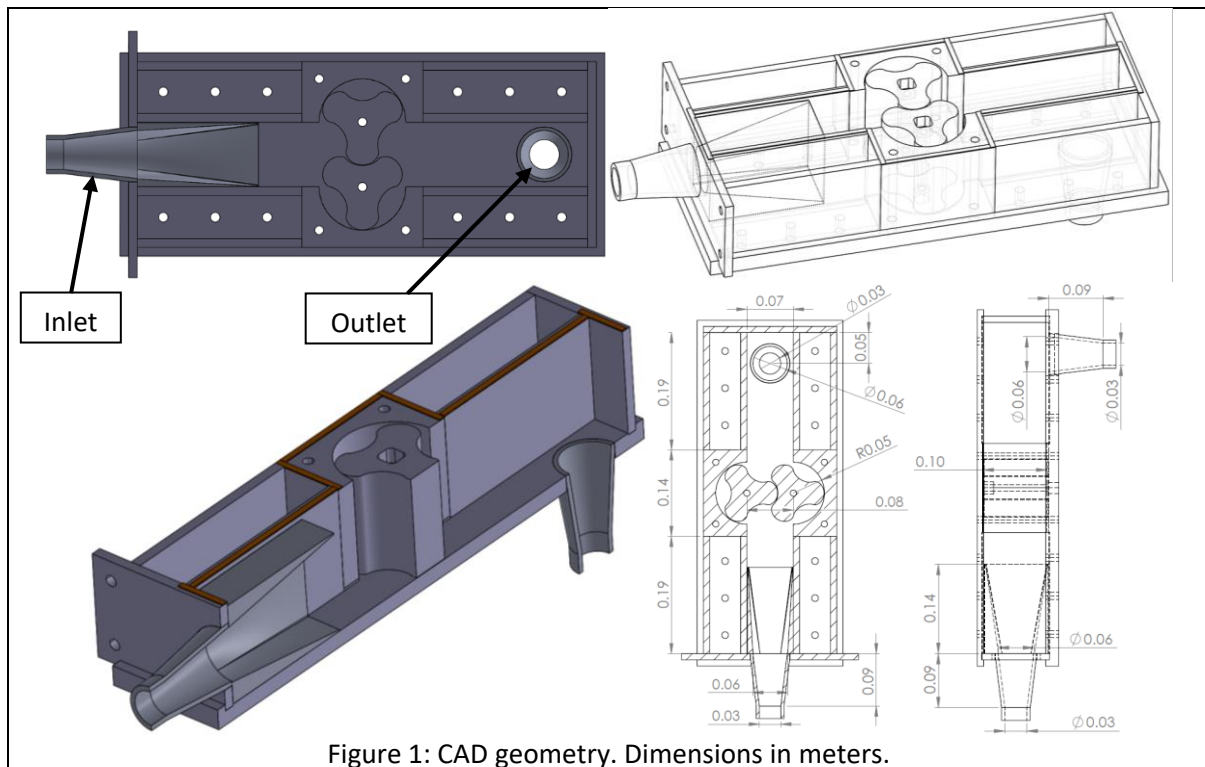
Section 2 presents the geometry and experimental set-up. Section 3 discusses the PIV results, with particular examples and references to the complete set of results shown in the appendix. Section 4 gives a short conclusion.

2. Geometry and experimental set-up

The design of the geometry and the rig was developed in collaboration with the group at NTNU. The group at NTNU is responsible for the CFD simulations that should later use the PIV results for validation. The collaboration ensured that the experiments were set up the best way.

Figure 1 shows the CAD geometry of the measurement section, including detailed dimensions. The lobe shape is based on mathematical functions that are provided through a Matlab script in Appendix A. The clearances between the rotor lobes and the top and bottom lids are approximately 0.5-1mm, given by a thin seal between those lids and the side walls (seen in red in Figure 1). The inlet and outlet diffusers were designed to get a more even velocity distribution for the PIV measurements. The outlet diffuser should preferably be designed the same way as the inlet diffuser, but the requirement of optical access for the PIV laser sheet forced the present design. The CAD file and the lobe Matlab script are supplied together with the data.

The test rig is a closed-loop system, as shown in Figure 2 and Figure 3, where the water goes from the bottom outlet of the test section, through an external pump, through a control valve, through a flow meter, and back to the inlet of the test section. The external pump drives the flow through the test section when operating in turbine mode and is not used when operating in pump mode. The control valve is used to set the required head when operating in pump mode and is not used when operating in turbine mode. The runner lobes are rotated by a motor and a gearbox that connects the rotation of the two rotors, making them rotate at exactly the same rotational speed but in opposite directions. An RPM sensor is used to monitor the rotational speed. Due to the small size of the test rig, the losses in the gear box and in the seals prevented the runner lobes from rotating in turbine mode, irrespectively of the head and flow rate. Thus, the motor had to be used also in turbine mode, to overcome those losses. This has no effect on the results of the PIV measurements, since the flow does not know if the runner lobes are rotating due to the forces from the flow or due to an external motor. The PIV results will give the velocity distributions under the conditions set in the experiments.



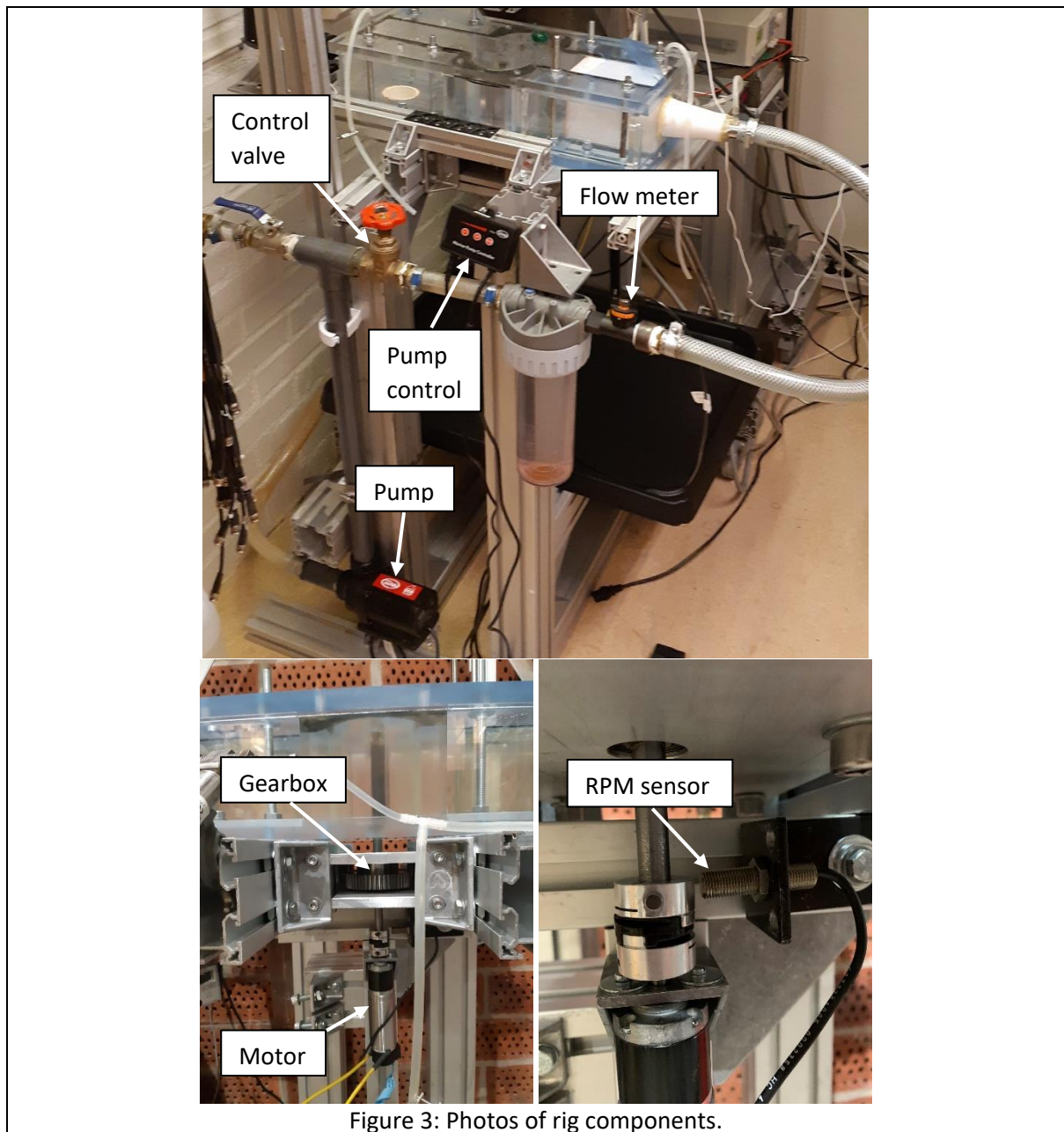


Figure 4 shows the inlet and outlet diffusers that were designed to get a more even flow distribution, and the static pressure measurement hoses to get the static pressure difference over the test section.

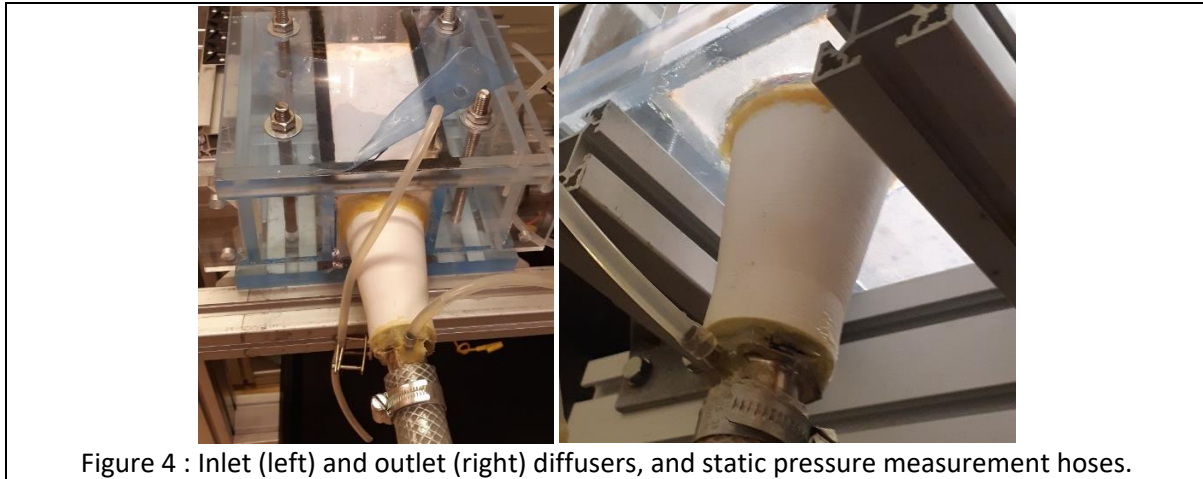


Figure 4 : Inlet (left) and outlet (right) diffusers, and static pressure measurement hoses.

Figure 5 shows the two-camera stereo PIV set-up, with a horizontal laser sheet at mid-height of the measurement section entering through the PIV lens at the left side of the pictures (see also Figure 2). One of the cameras (right) is positioned perpendicular to the measurement plane and another camera (left) is positioned at an angle of 30° with respect to the vertical axis (for outlet measurements). This way it was possible to use the first camera for 2D-2C (two-dimensional, two-component) measurements and the two cameras together were used for 2D-3C (two-dimensional, three-component) for the outlet measurements. The cameras are 14-bit Imager Pro X 4 M with a 2048×2048 pixel sensor and $7.4 \mu\text{m}$ pixel dimension. The camera lenses (105-mm f/2.8 Sigma) were equipped with 570-nm low-pass filters to separate the fluorescent emission of the particles and the laser illumination. The planar illumination was performed by EverGreen 200 dual-cavity Nd-YAG laser with 532 nm wavelength. The laser was equipped with light-sheet forming optics, generating a horizontal light sheet with a thickness 2-3 mm. The fluid was regular tap water, which was found to have a sufficient index-matching with the transparent PMMA materials for the requested horizontal PIV plane through the test section. The laser sheet was able to penetrate the entire measurement section, including the runner lobes, without refractions out of the measurement plane. The water was seeded with 20- μm fluorescent Rhodamine B-based polystyrene particles. The fluorescent PIV was employed to avoid reflections from the metallic parts of the rig. The PIV calibration was carried out in situ, by placing a 2-plane calibration target inside the rig filled with water.

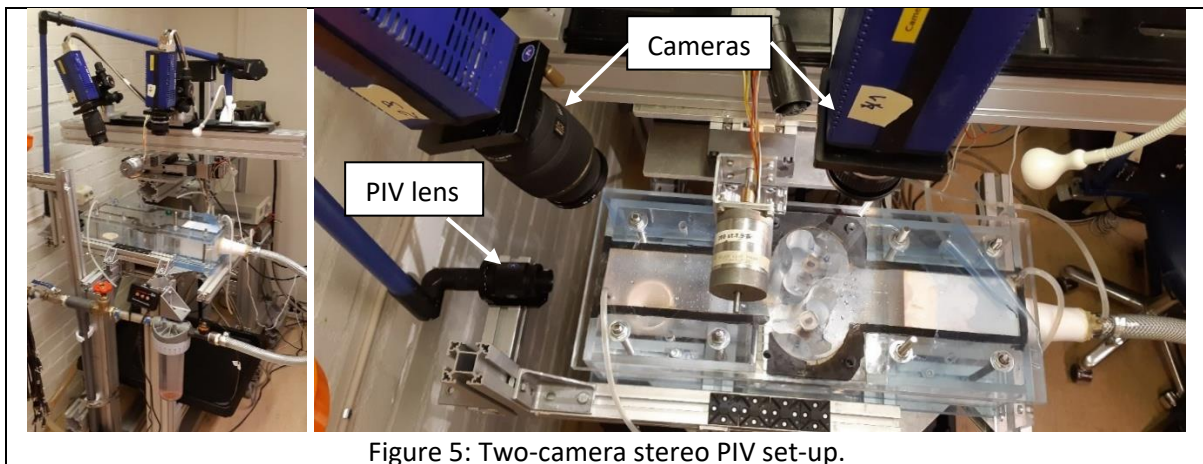


Figure 5: Two-camera stereo PIV set-up.

The synchronization of the PIV system with the rotation of the rotor lobes was performed using a Hall effect sensor and a magnet mounted on the shaft of the motor, see Figure 3. An example of a particle image from one of the cameras is shown in Figure 6. The Davis 10 PIV software from

LaVision was used for PIV processing. The processing steps included initial calibration with the calibration target, stereo self-calibration, stereoscopic reconstruction, cross-correlation and vector validation, vector statistics, and finally data masking. Velocity component statistics is obtained by phase-averaging of 100 images. The cross-correlation was performed in multipass procedure with decreasing window size in half. Initial interrogation window size was 64×64 pixels with 50 % overlap and final pass was performed with 32×32 pixels area size, 75 % overlap. The distances between each measurement point in both x and y directions for the full view, inlet and outlet measurement regions (see Figure 7) were approximately 0.795mm, 0.454mm and 0.292mm, respectively.

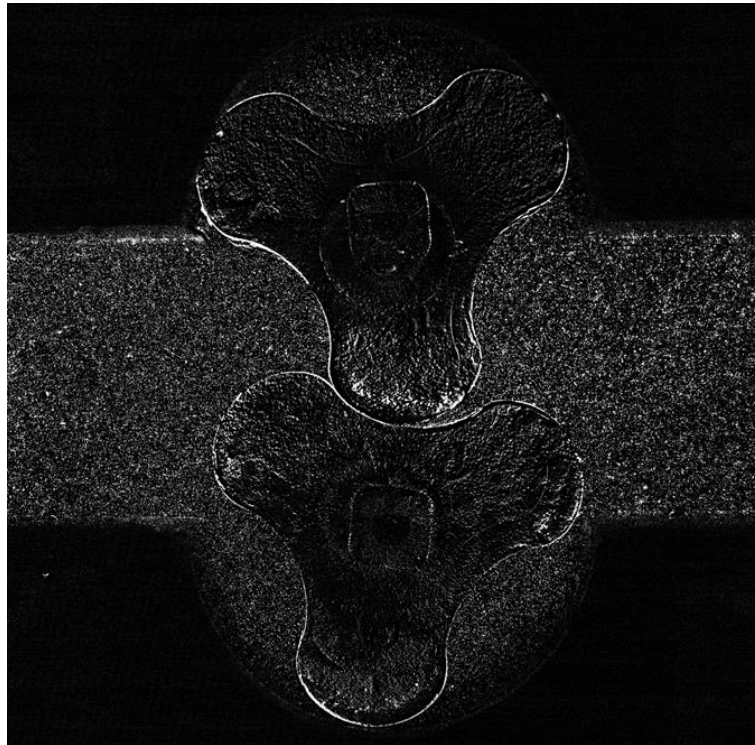


Figure 6: Example of particle image. It should be noted that the measurement plane is located at mid-height of the lobes, and that perspective makes it look like the upper lobe extends outside the channel. PIV can only measure what is visible, so the lobes also cover some of the flow. This effect can be seen in all the results. The upper lobe rotates clockwise and the lower lobe rotates counter-clockwise.

Table 1 shows global details of the investigated cases, including revolutions per minute (RPM), flow rate (in liters per minute (LPM) and m^3/s) and pressure difference. The total and static pressure differences are the same since the inlet and outlet pipes were of the same cross-section area. It should particularly be noticed that the flow rate in turbine mode is about 2.7 times larger than in pump mode for the same rotational speed, which is discussed in the following.

Table 1: Global details of investigated cases					
Case	RPM	Flow, LPM	Flow, m^3/s	dP, Pa	dP tot, Pa
Pump 45 RPM	45	11	1.83E-04	1058	1058
Pump 55 RPM	55	13	2.17E-04	1230	1230
Turbine 45 RPM	45	29.3	4.88E-04	-858	-858

An ideal positive-displacement reversible pump-turbine without any leakage should have exactly the same flow rate in both modes for the same rotational speed. Such an ideal flow rate would be based on the volume of water entrapped between the lobe and the housing and the rotational speed. The volume of water entrapped between the lobe and the housing can be calculated from the equations governing the lobe shape and a circle with a radius of the outer radius of the lobe (see Appendix D, which includes links to definitions and derivations). Neglecting the volume due to the clearance is appropriate for the ideal case of zero clearance. The area of an epicycloid is given by

$$A_{epi} = (k + 1)(k + 2)\pi r^2,$$

where k is the number of cusps and r is the radius of the small circle that forms the shape. The area of a hypocycloid is given by

$$A_{hypo} = (k - 1)(k - 2)\pi r^2.$$

A lobe is constructed from one half of a full epicycloid and one half of a full hypocycloid. Thus, the area of a lobe is given by $A_{lobe} = (A_{epi} + A_{hypo})/2$.

The area of a circle with a radius of the outer radius of the lobe is given by

$$A_{circ} = \pi R^2,$$

where $R = r(k + 2)$. Thus, the area between the lobe and the circle with a radius of the outer radius is given by

$$A = ((k + 2)^2 - \frac{(k+1)(k+2)+(k-1)(k-2)}{2})\pi r^2 = (4k + 2)\pi r^2.$$

In our case, $k = 6$, and an outer lobe diameter of 0.1m gives $R = 0.05$. Thus, $r = R/(k + 2) = 0.05/(6 + 2) = 0.00625$, so $A = 0.00319 \text{ m}^2$. The volume is given by this area times the height, i.e $V = 0.00319 * 0.1 = 0.000319 \text{ m}^3$. This is the volume transported by each lobe each lap, and since we have two lobes the total volume transported per lap is $V_{lap} = 0.000638 \text{ m}^3 = 0.638 \text{ L}$. For 45 RPM during one minute, the total transported volume is $V_{lap} * 45 = 28.72 \text{ LPM}$. Comparing this to Table 1, it can be seen that the turbine mode has a higher flow rate than the theoretical, which is caused by the water being pushed through the clearances in the same direction as the transport of water due to the rotating lobes. The pump mode operating at 45 RPM has a significantly reduced flow rate due to the opposing pressure gradient that pushes the water through the clearances in the opposite direction compared to the transport of water due to the rotating lobes. At the same time it should be noted that the pressure difference is different between the measured turbine and pump modes, yielding a higher adverse leakage flow in pump mode.

3. PIV results

Table 2 shows a summary of the PIV results, as they are organized in the file folder. For each of the three regions “Full view”, “Inlet” and “Outlet”, three phase angles were measured. The phase angles are named “0”, “15” and “30” in the file folder, which corresponds to the angle relative to the first phase angle of that region. Those angle notations are used when showing all results. The true angle is given in brackets in the same column of the table. The angle is for the lobe visualized with a thick line in Figure 7, where zero degrees is straight to the left and a positive angle is along the clockwise direction. Note that perspective view makes it look like the lobes are partly outside the flow region, since the green plane is at mid-height of the rotors. For each measurement region and each phase, each of the three cases are measured.

Table 2: Summary of PIV results, as in file folder. Phase angles in quotation marks are with respect to the first phase angle of that region. Phase angles in brackets are actual angles.		
Region	Phase	Case
Full view	“0” (-7)	Pump 45 RPM
		Pump 55 RPM
		Turbine 45 RPM
	“15” (8)	Pump 45 RPM
		Pump 55 RPM
		Turbine 45 RPM
	“30” (23)	Pump 45 RPM
		Pump 55 RPM
		Turbine 45 RPM
Inlet	“0” (-11)	Pump 45 RPM
		Pump 55 RPM
		Turbine 45 RPM
	“15” (4)	Pump 45 RPM
		Pump 55 RPM
		Turbine 45 RPM
	“30” (19)	Pump 45 RPM
		Pump 55 RPM
		Turbine 45 RPM
Outlet	“0” (188)	Pump 45 RPM
		Pump 55 RPM
		Turbine 45 RPM
	“15” (203)	Pump 45 RPM
		Pump 55 RPM
		Turbine 45 RPM
	“30” (218)	Pump 45 RPM
		Pump 55 RPM
		Turbine 45 RPM

Table 2 sums up to 27 folders, each with 100 instantaneous PIV snapshots, or a total of 2700 PIV snapshots. Each snapshot contains data for the U and V velocity components, and also the W component for the Outlet region. Each line in each file contains the x-position, y-position, U-component, V-component (and W-component for the Outlet regions), for each measurement point in the PIV data.

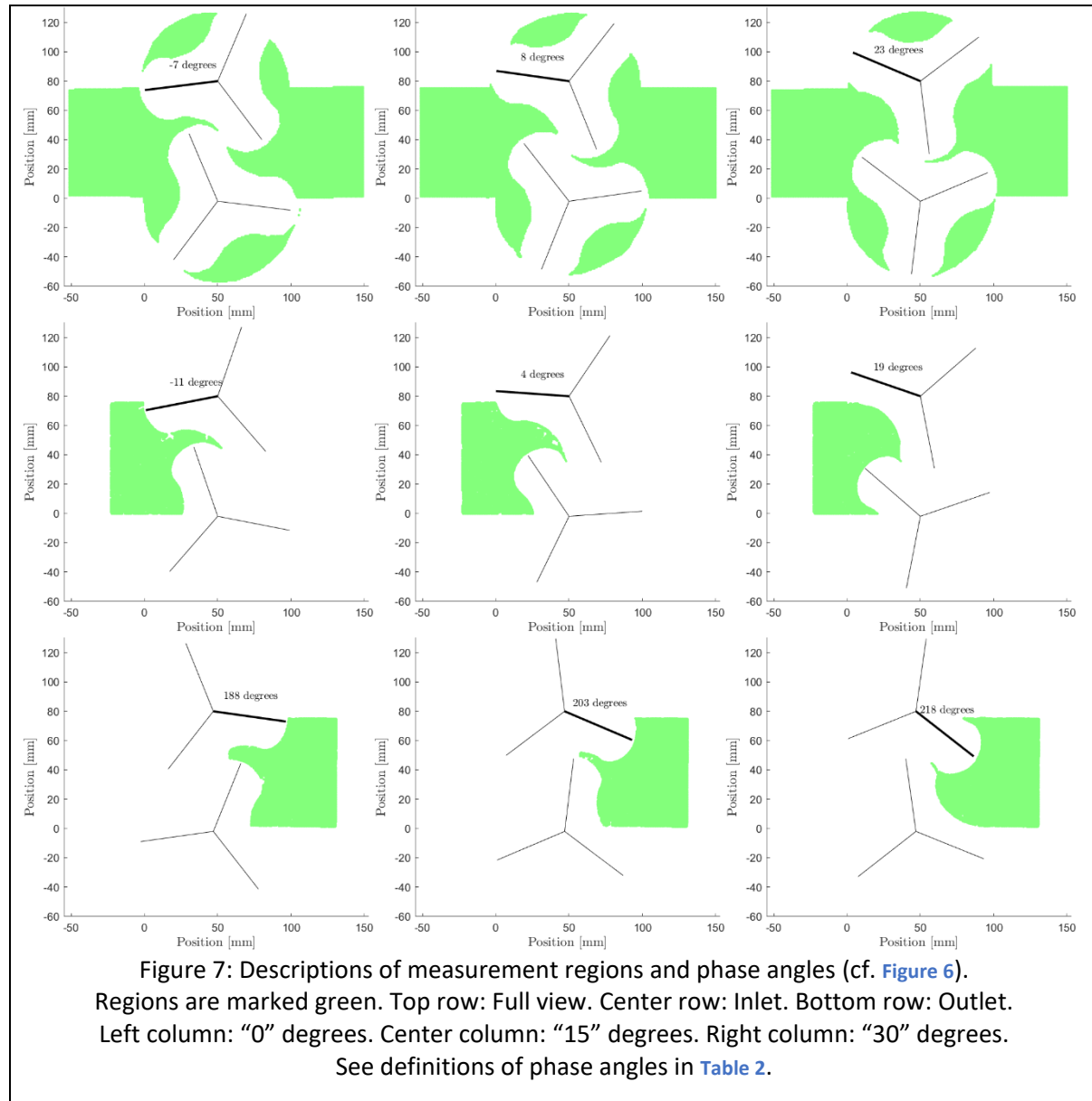


Figure 8 shows examples of snapshots of instantaneous U and V velocity components for full view at phase angle "0" degrees, for all three cases. A total of 2700 snapshots for each of the U and V velocity components and 900 snapshots for the W velocity component are available, but not shown here to save space. A positive U-component denotes a flow from left to right in all images, and a positive V-component denotes a flow from bottom to top in all images. From the signs of the velocity components (particularly the V component), it is obvious that the upper lobe is rotating clockwise and the lower lobe is rotating counter-clockwise. The instantaneous views give an indication of the flow unsteadiness as well as an indication of the main regions of different velocity magnitudes. In particular it can be seen that the turbine mode has a region of large U-velocity values

at the center of the outlet channel, which is not seen in pump mode. This will be discussed more later. For main flow features it is better to consider the phase-averaged velocity components, which is the average of all instantaneous fields for a particular phase angle. The standard deviation of the same data, on the other hand, gives a measure of the instantaneous deviation from the phase-averaged values.

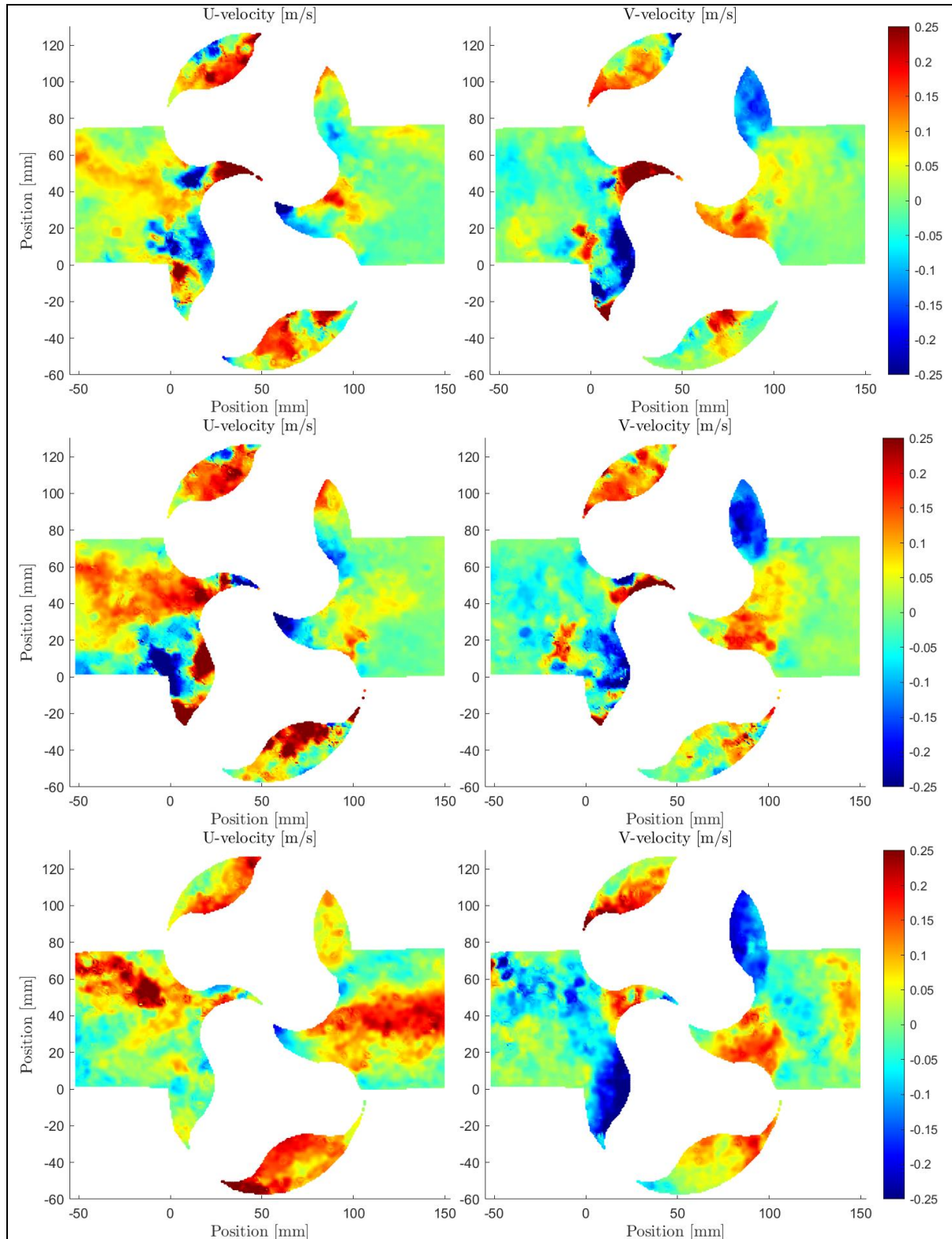


Figure 8: Full view, examples of instantaneous velocity components at “0” degrees. Left: U-velocity. Right: V-velocity. Top: Pump 45 RPM. Center: Pump 55 RPM. Bottom: Turbine 45 RPM.

Appendices B and C provide a complete set of all the contour plots of phase-averaged U and V velocity components for “Full view”, “Inlet” and “Outlet” and W velocity component for “Outlet”, for all cases and all phase angles. Appendix D shows examples of standard deviation of the data used for the phase-averaging, indicating regions where the velocity components instantaneously differ considerably from the phase-averaged values. Some of the results are discussed in the following.

Figure 9 shows the phase-averaged U and V velocity components for the full view and phase angle “0” degrees for all cases (taken from Appendix B). The instantaneous velocity components in Figure 8 constitutes one of the 100 samples used for each of these averages. Appendix D shows the corresponding standard deviations. It can be seen in the chambers (the closed confined regions between the lobes and the housing) that the flow velocity tends to be higher at a lower lobe radius, both in the U and V components. It can also be seen in the V-component at the upstream side of the lower lobe that a clockwise vortex is forming already long before the chamber is closed. This vortex is likely to be maintained throughout the passage of the chamber, as observed and discussed before. The same should happen for the other lobe, forming a counter-clockwise vortex, although that phase angle is not included in the measurements.

There is a region of higher U-velocities at the center (slightly biased upward in the pictures) of the inlet channel in pump mode and at the upper side of the inlet channel in turbine mode. It can’t be seen from the experimental data if the location of this increased velocity depends on the lobe angle, since the corresponding “0” degree angle for the lower lobe was not included in the measurements. Thus, it remains to be studied if the same effects can also be seen in CFD, if it moves between the sides, and if so, find a reason for it. It may potentially be caused by imperfections in the experiments. There may for instance be a tiny difference in clearances for the two lobes, causing the flow to prefer a particular side. In turbine mode, the pressure difference pushes the flow from left to right (inlet to outlet), which may amplify this effect compared to pump mode, where it is the lobes that drive the flow. It should be remembered that although the flow is in the same direction for pump and turbine mode in these experiments, the pressure gradient is opposite in pump and turbine mode.

As briefly discussed for the instantaneous results, a particular difference between the pump and turbine modes occurs also in the phase-averaged results in the outlet channel, as seen in Figure 9. A strong U-velocity is formed in the center of the outlet channel in turbine mode. It has a wavy structure that corresponds to the flow rate and the lobe rotational speed. The wavy structure can also be seen by carefully investigating the V-velocity in the same region, which shows a shedding behaviour. To further investigate the cause of this effect in turbine mode, Figure 10, Figure 11 and Figure 12 visualize the U-velocity, V-velocity and velocity vectors in the outlet region. A sequence of six phase angles is shown by using both the data from the outlet measurements and zooms of the full view measurements. It could be argued that the origin of this effect may be due to leakage between the lobes, but then also some increased U-velocity should be seen in that clearance. This can’t be observed in the results, so that can’t be the reason. Instead, it can be seen that there is a strong V-velocity in the chamber as it opens to the outlet side. It forms a jet-like structure towards the center of the channel that causes the flow to separate from the side walls and move towards the center. At the center, this jet interacts with the jet that previously came from the other side, as well as a jet that comes from the squeezed water between the lobes. This all together forms a large and

periodically fluctuating U-velocity at the center of the outlet channel. It can be seen in Figure 9 that the flow in the chambers differ slightly between pump and turbine mode. In particular, the V-velocity is slightly lower in pump mode at the point where these chambers open to the outlet. It can also be seen that the U-velocity is larger in the lower chamber in turbine mode. This could be caused by additional leakage between the lobes and the housing in turbine mode. This is indicated in the results in turbine mode. At the lower end of the lower lobe an increased U-velocity is observed at the downstream side of the clearance. At the left side of the upper lobe an increased V-velocity is observed at the downstream side of the clearance. This indicates an elevated leakage flow between the lobes and the housing in turbine mode. It can also be seen that the flow in the chamber of the lower lobe is influenced by this leakage, which leads to the effects seen downstream the lobes in turbine mode. Finally, another difference between pump mode and turbine mode is that the flow after the lobes is pushed by the lobes to the outlet in pump mode and sucked by the outlet in turbine mode. This may cause a difference in how the water is transported from the lobes to the outlet. This was not investigated in the experiment but should easily be possible to investigate by CFD.

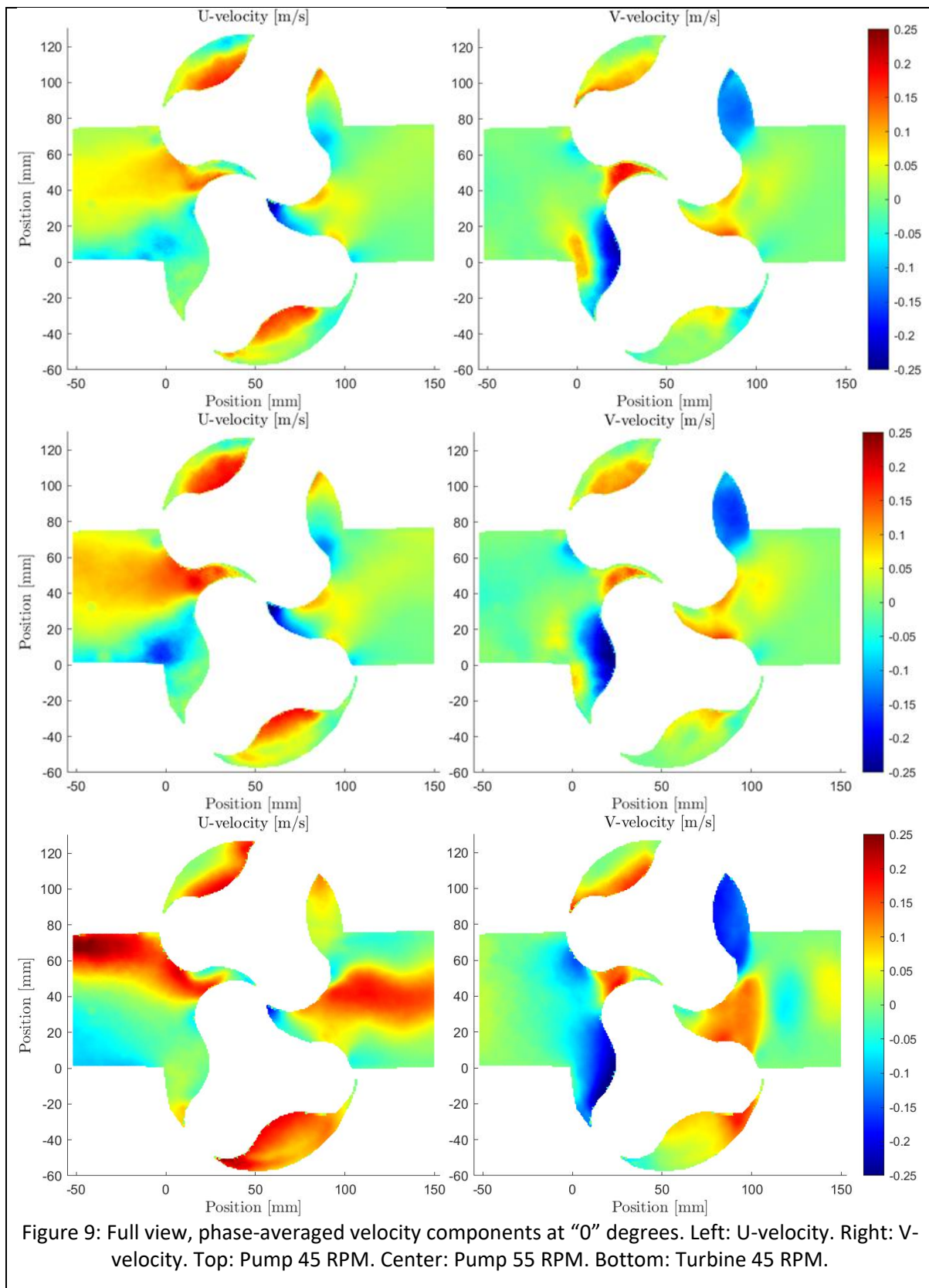


Figure 9: Full view, phase-averaged velocity components at "0" degrees. Left: U-velocity. Right: V-velocity. Top: Pump 45 RPM. Center: Pump 55 RPM. Bottom: Turbine 45 RPM.

In Appendix D it can be seen that the largest standard deviations typically occur in regions where the flow is influenced by the interaction between the lobes and between each lobe and the housing. It makes sense that as the water is squeezed between different walls, there may be jet-like structures trying to escape in all directions. In pump mode, the standard deviation also has increased values where the previously discussed vortex in the chambers (before they are closed) is formed and where the flow goes over a backward facing step. In turbine mode, the standard deviation increases in the region of increased U-velocity in the inlet channel.

4. Conclusions

An experimental rig for studies of the flow in a positive-displacement reversible pump-turbine has been designed, manufactured, assembled and thoroughly described. Comprehensive PIV measurements at mid-height of the lobes have been made, with additional high-resolution measurements at the inlet and outlet of the lobes. The U and V-velocity components have been recorded in the full measurement domain, and also the W-velocity has been recorded at the outlet of the lobes. The data has been collected for specific lobe phase angles, allowing phase averaging and determination of the standard deviation of the flow at those particular phase angles. All the phase-averaged U, V and W-velocities have been visualized, as well as examples of instantaneous snapshots and standard deviation. Although the most important deliverable of the work is the actual data, to be used in later CFD validation, some main features of the flow have been discussed. It has particularly been shown that the flow in the chambers tends to contain a large vortical structure. That vortical structure is initiated at a phase long before the chamber is closed. The flow in the chamber in pump mode is influenced by an increased leakage between the lobes and the housing. Further, a couple of significant differences between the flow in pump mode and turbine mode have been identified. The flow in turbine mode has shown imperfections in both the inlet and outlet channels. A strong jet-like flow appears at the center of the outlet channel in turbine mode. It has been discussed that this is related to the higher flow rate in turbine mode, and an increased leakage flow between the lobes and the housing. The difference in leakage flow between pump and turbine modes is related to the pressure gradient. In pump-mode, the lobes are pushing the flow against the pressure gradient. In turbine mode, the lobes are being pushed by the pressure gradient. In pump mode, the lobes are sucking the flow from the inlet. In turbine mode, the flow is pushed from the inlet hose. In pump mode, the lobes are pushing the flow towards the outlet. In turbine mode, the flow is sucked to the outlet by the outlet hose. This seems to yield a higher sensitivity of the experimental setup in turbine mode, which must however be verified by tests using CFD, where it is much easier to investigate different designs of inlets and outlets.

All the experimental data shown in this report, together with the Matlab post-processing scripts, have been made openly available through storage in the open access 4TU repository for validation of CFD and further studies using CFD. That is the most important outcome of the deliverable.

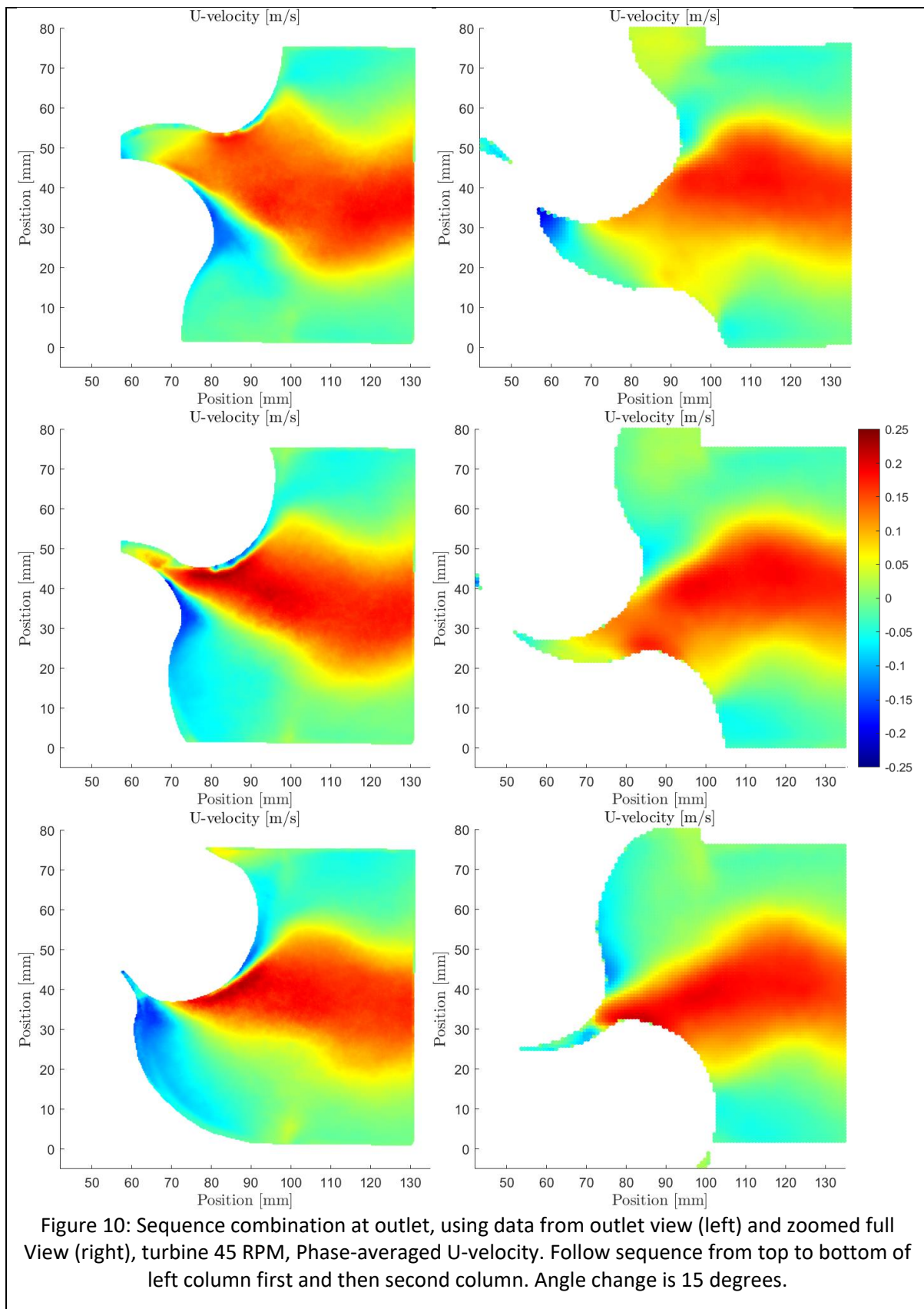
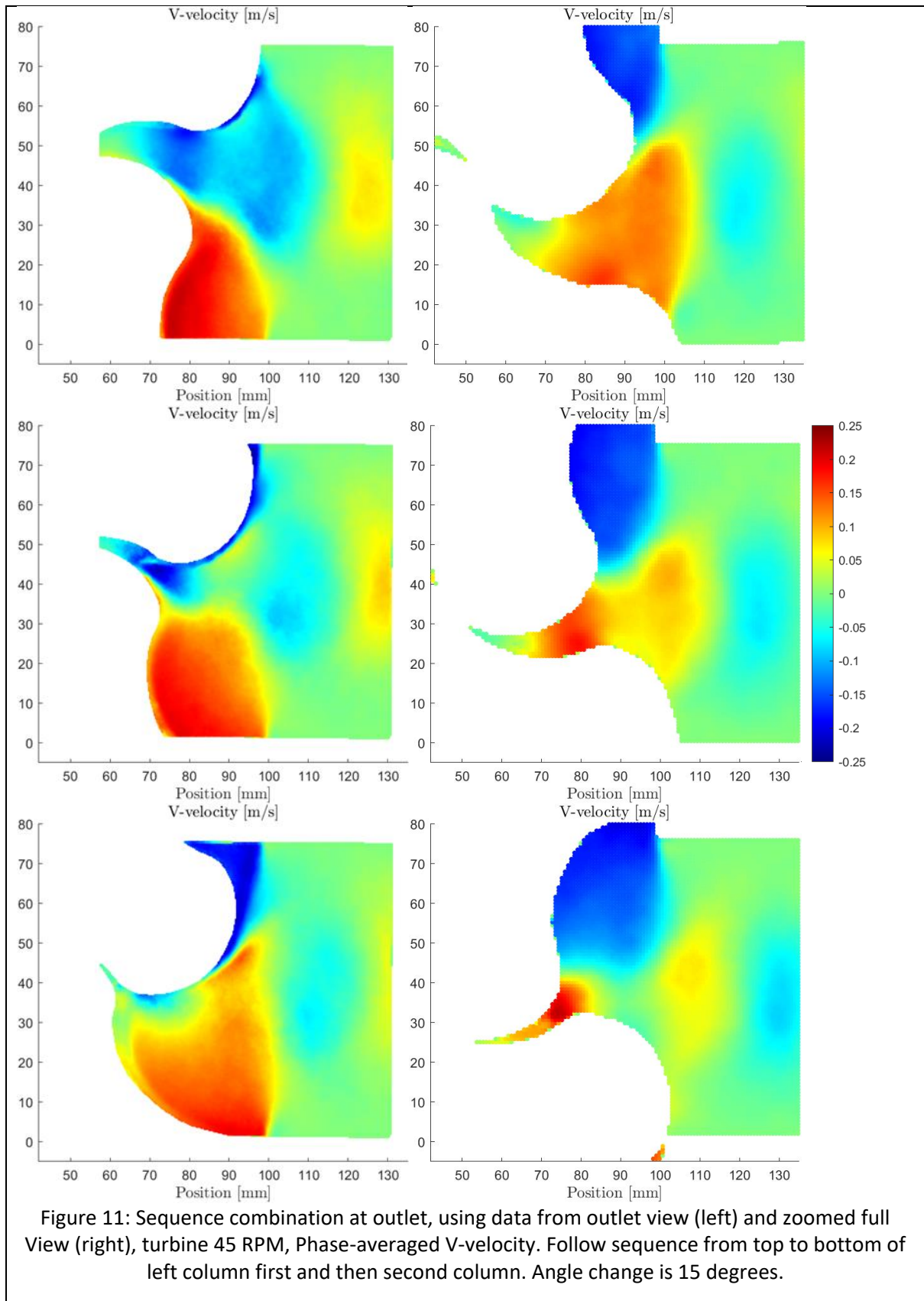
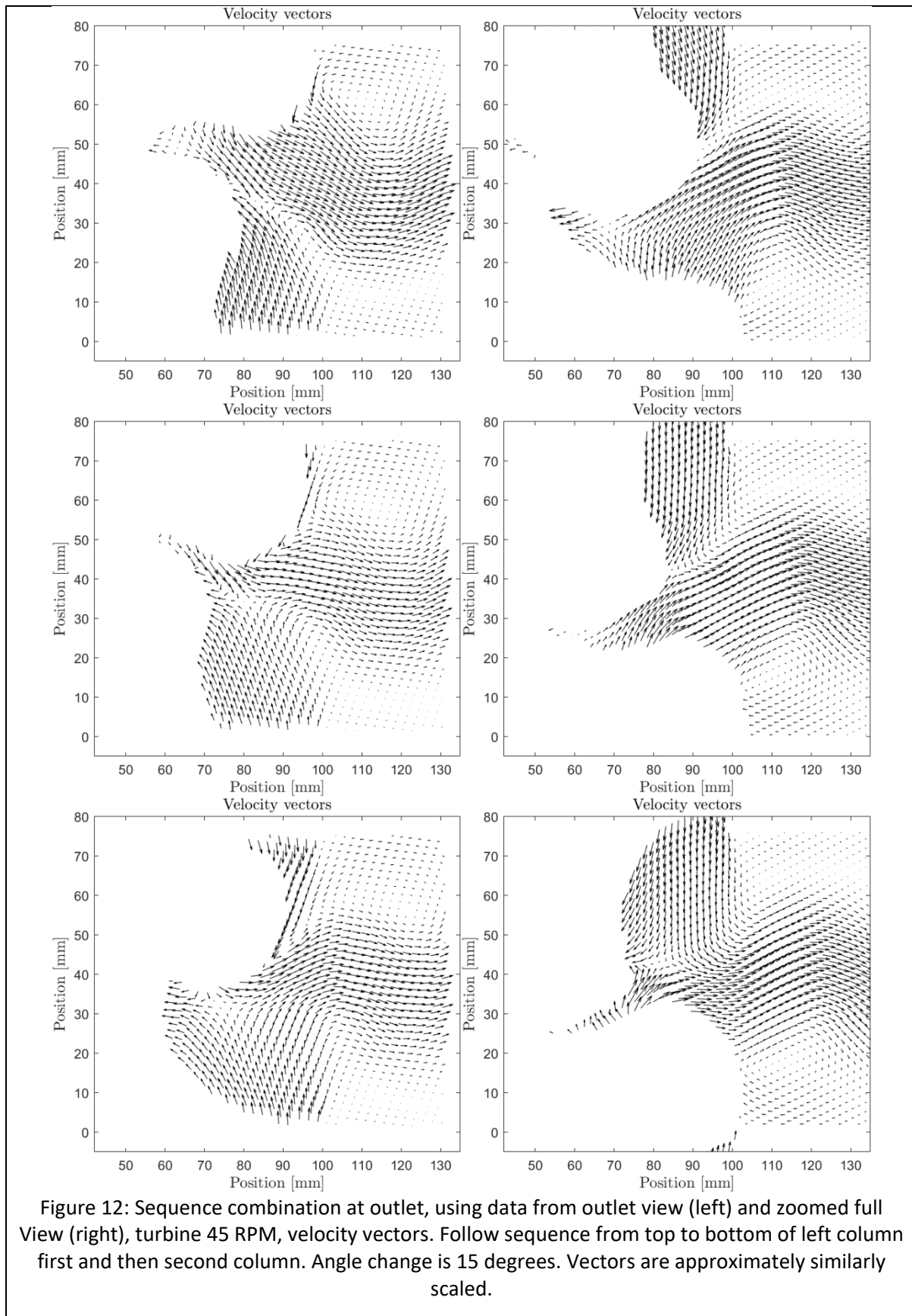


Figure 10: Sequence combination at outlet, using data from outlet view (left) and zoomed full View (right), turbine 45 RPM, Phase-averaged U-velocity. Follow sequence from top to bottom of left column first and then second column. Angle change is 15 degrees.





Appendix A: Lobe geometry

Matlab script for lobe geometry, followed by its plot.

```
%Script to plot lobe shape
%Sequence of epi-and hypo-cycloid curves,
%here varying from
%epi: 0 to pi/3, 2*pi/3 to 3*pi/3 and 4*pi/3 to 5*pi/3
%hypo: pi/3 to 2*pi/3, 3*pi/3 to 4*pi/3 and 5*pi/3 to 2*pi
%https://en.wikipedia.org/wiki/Hypocycloid
%https://en.wikipedia.org/wiki/Epicycloid

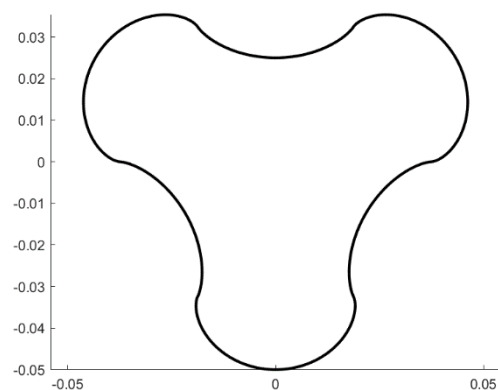
clear all
close all

D = 0.1; %Outer diameter
m = 3;   %Number of lobes (must be 2 or more, here 3)
k = 2*m; %Number of cusps (see links)
r = D/(2*(k+2));

anglespan = 0:pi/m/100:pi/m;
x_epi = zeros(m,length(anglespan));
y_epi = zeros(m,length(anglespan));
x_hypo = zeros(m,length(anglespan));
y_hypo = zeros(m,length(anglespan));

for i = 1:m
    t = anglespan+(i-1)*2*pi/m;
    x_epi(i,:) = r*(((k+1)*cos(t))-cos((k+1)*t));
    y_epi(i,:) = r*(((k+1)*sin(t))-sin((k+1)*t));
    x_hypo(i,:) = r*(((k-1)*cos(t+pi/m))+cos((k-1)*(t+pi/m)));
    y_hypo(i,:) = r*(((k-1)*sin(t+pi/m))-sin((k-1)*(t+pi/m)));
end

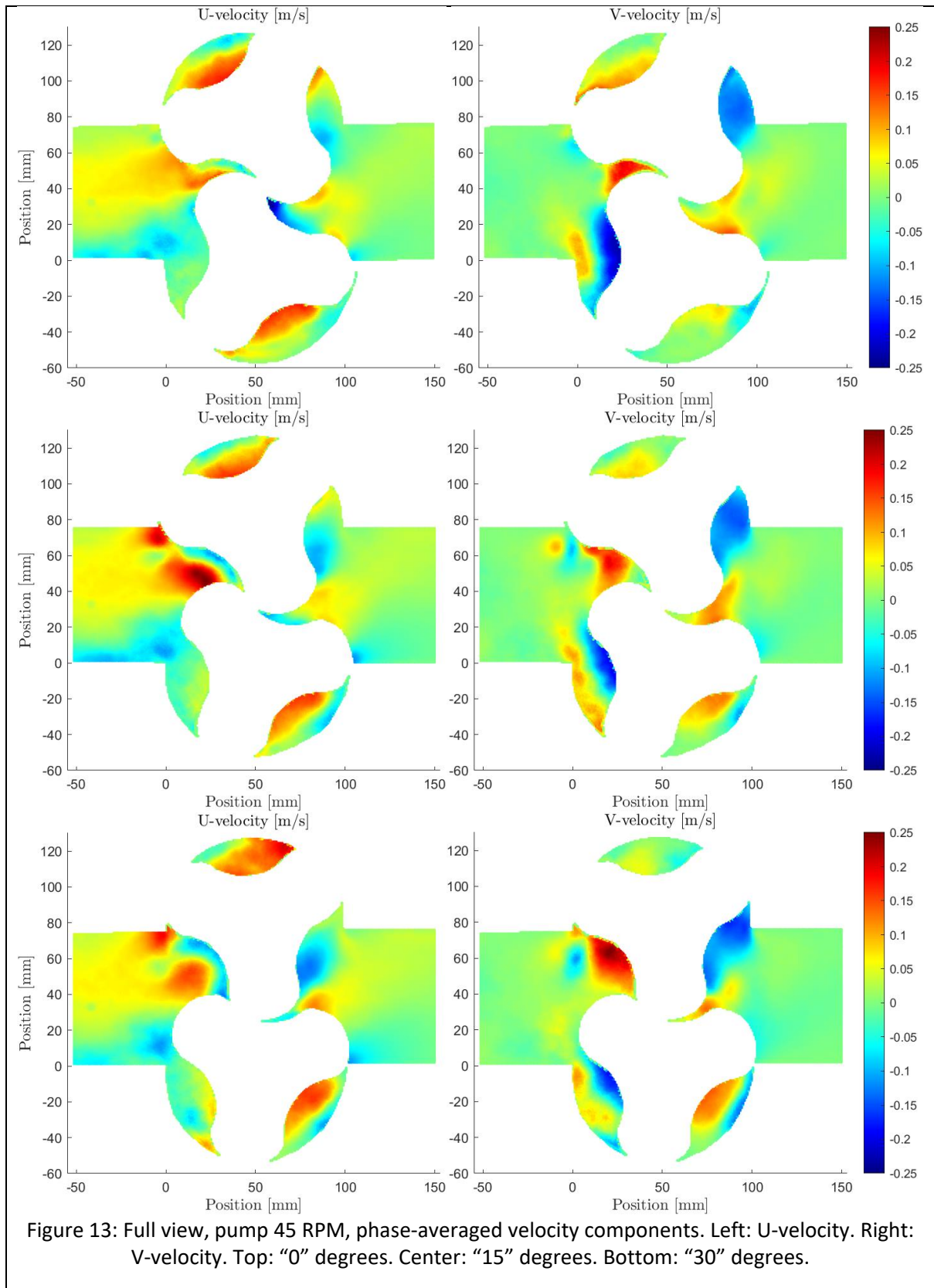
figure
hold on
for i = 1:m
    plot(x_epi(i,:),y_epi(i:), 'k', 'linewidth', 2)
    plot(x_hypo(i,:),y_hypo(i:), 'k', 'linewidth', 2)
end
%Check that D corresponds to outer diameter:
%p = nsidedpoly(1000, 'Center', [0 0], 'Radius', D/2);
%plot(p)
axis equal
%axis off
exportgraphics(gcf, "lobe_shape.png")
```

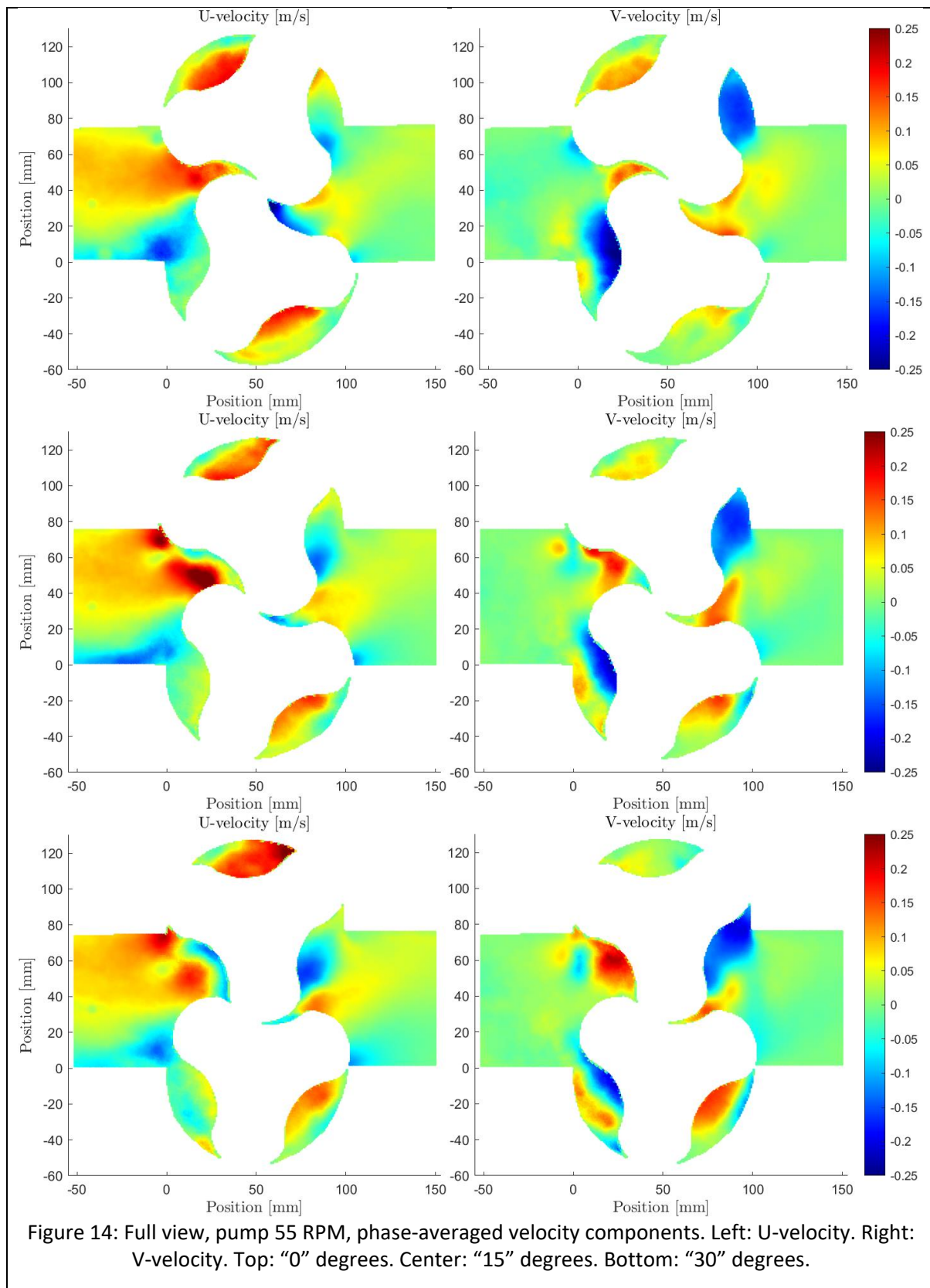


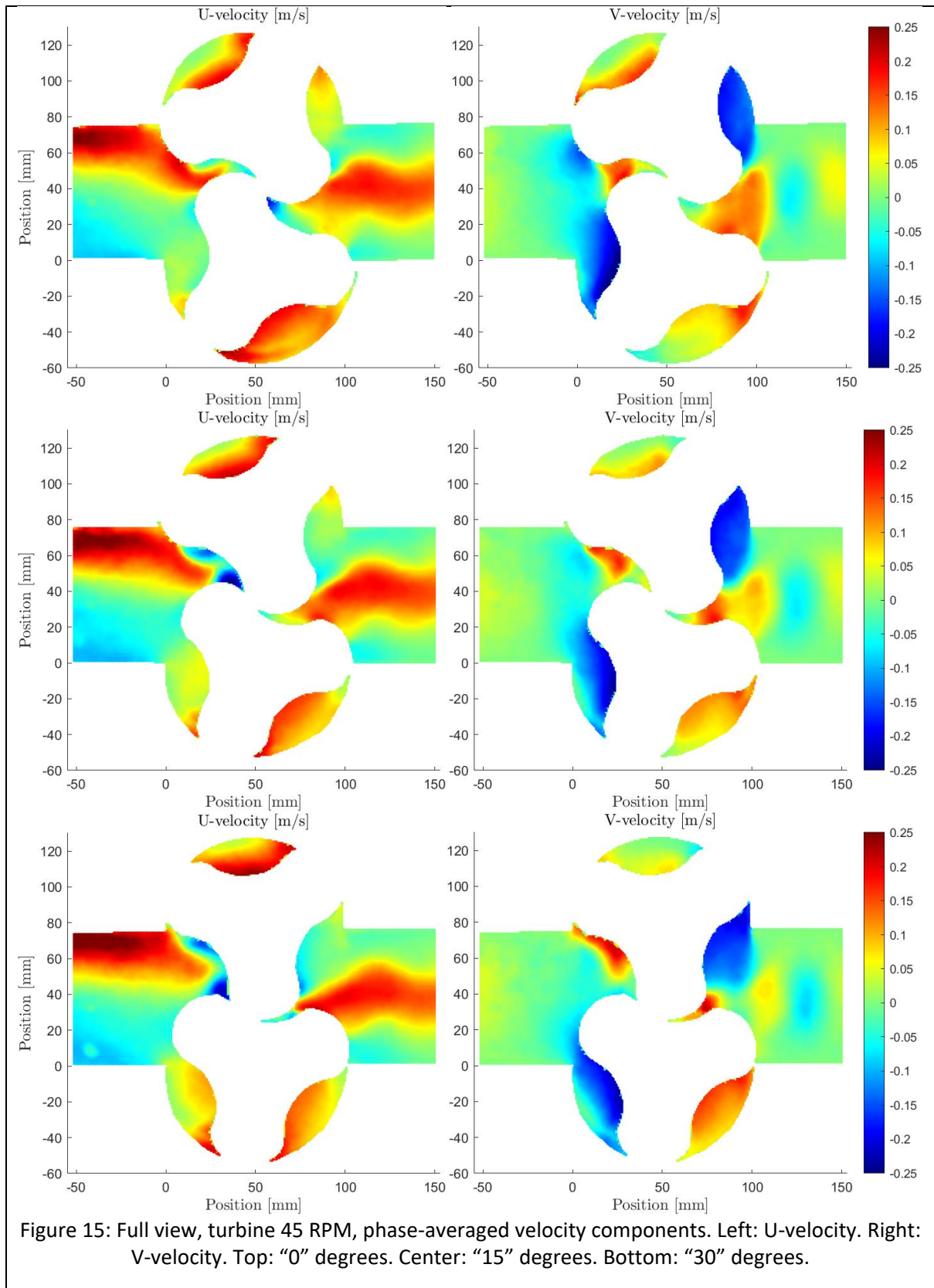
Appendix B: Contour plots of phase-averaged U and V velocity components

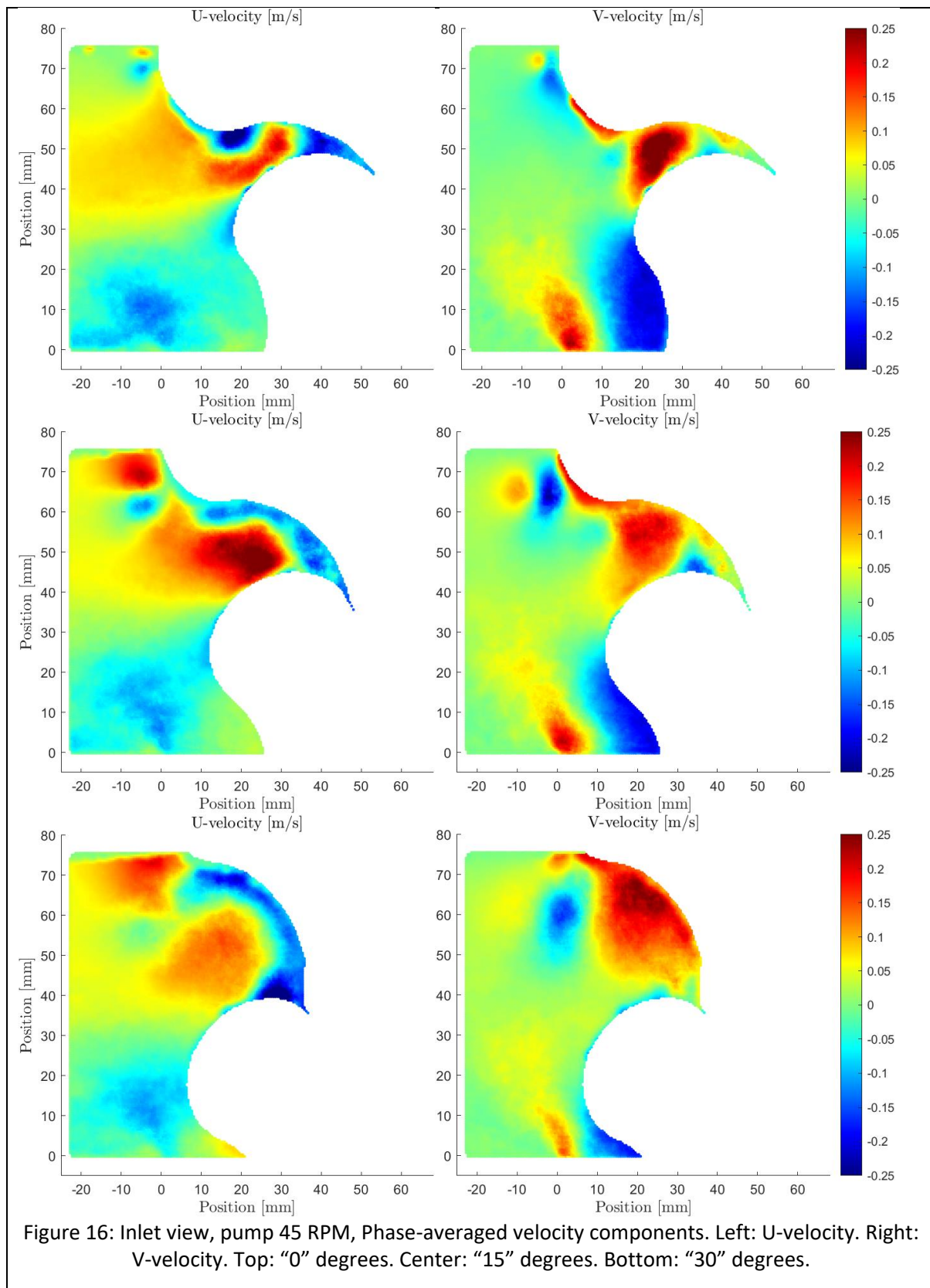
The figures presented here show all the contour plots of phase-averaged U and V velocity components for pump mode at 45 RPM, pump mode at 55 RPM, and turbine mode at 45 RPM. A positive U-component denotes a flow from left to right in all images, and a positive V-component denotes a flow from bottom to top in all images. For each case, three phase averaging angles are shown. The upper and lower runner lobes in the images are rotating in the clockwise and anti-clockwise, respectively, in both turbine and pump mode. The only difference is if the pressure difference between the inlet and outlet is supporting or counteracting the flow.

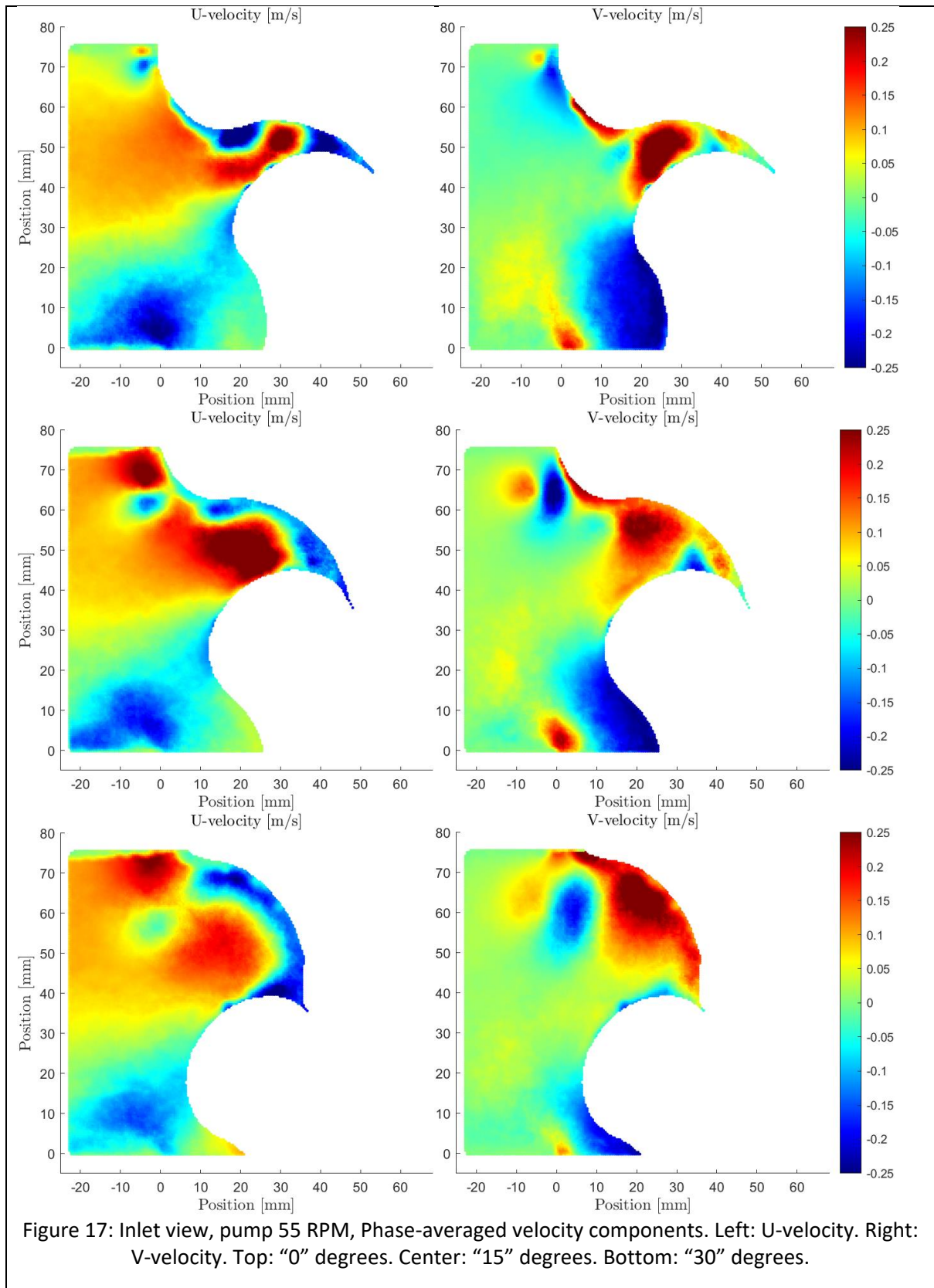
- Figures 13-15 show the results from the full view measurements.
- Figures 16-18 show the results from the inlet measurements with higher resolution.
- Figures 19-21 show the results from the outlet measurements with higher resolution.

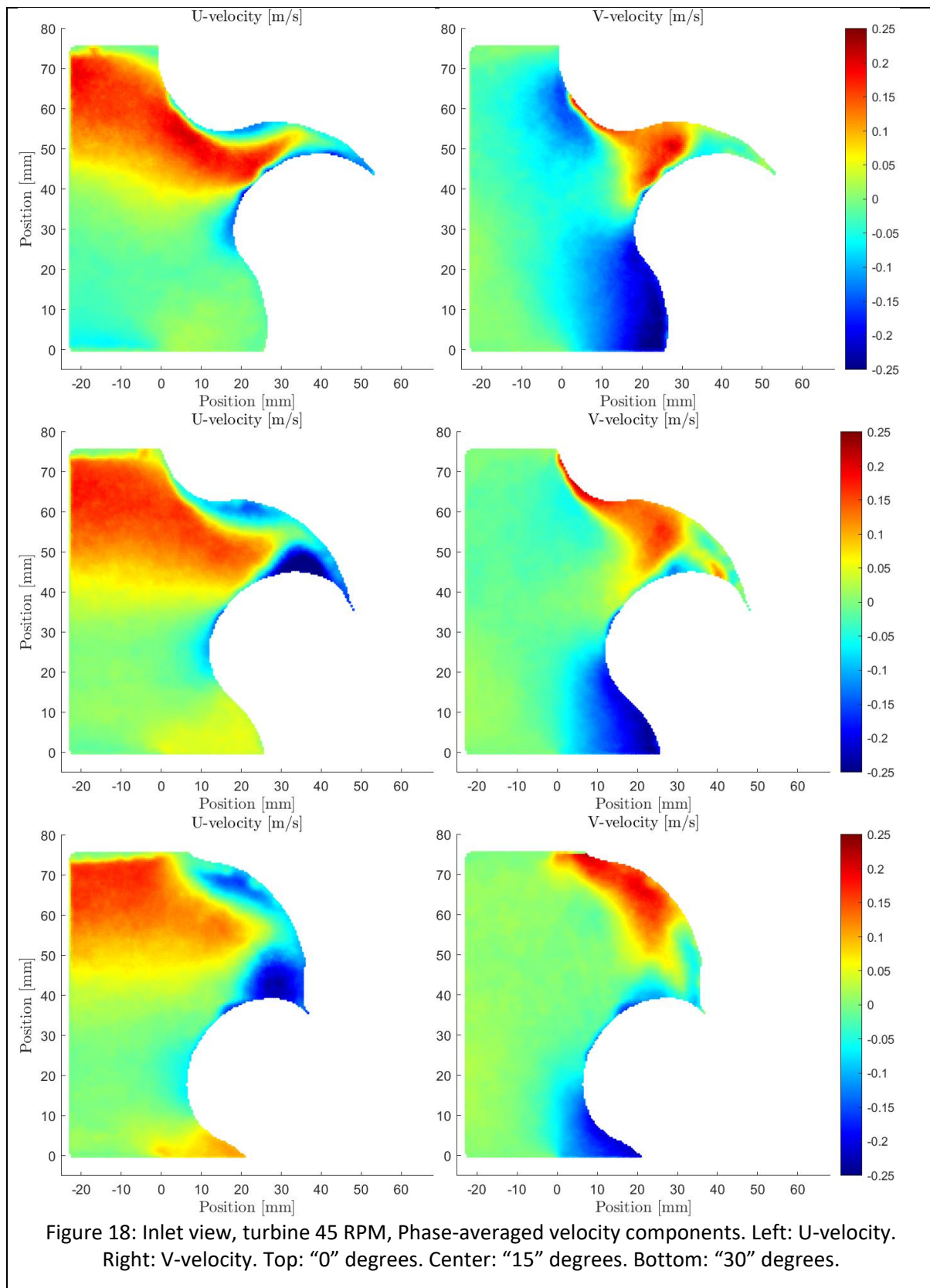


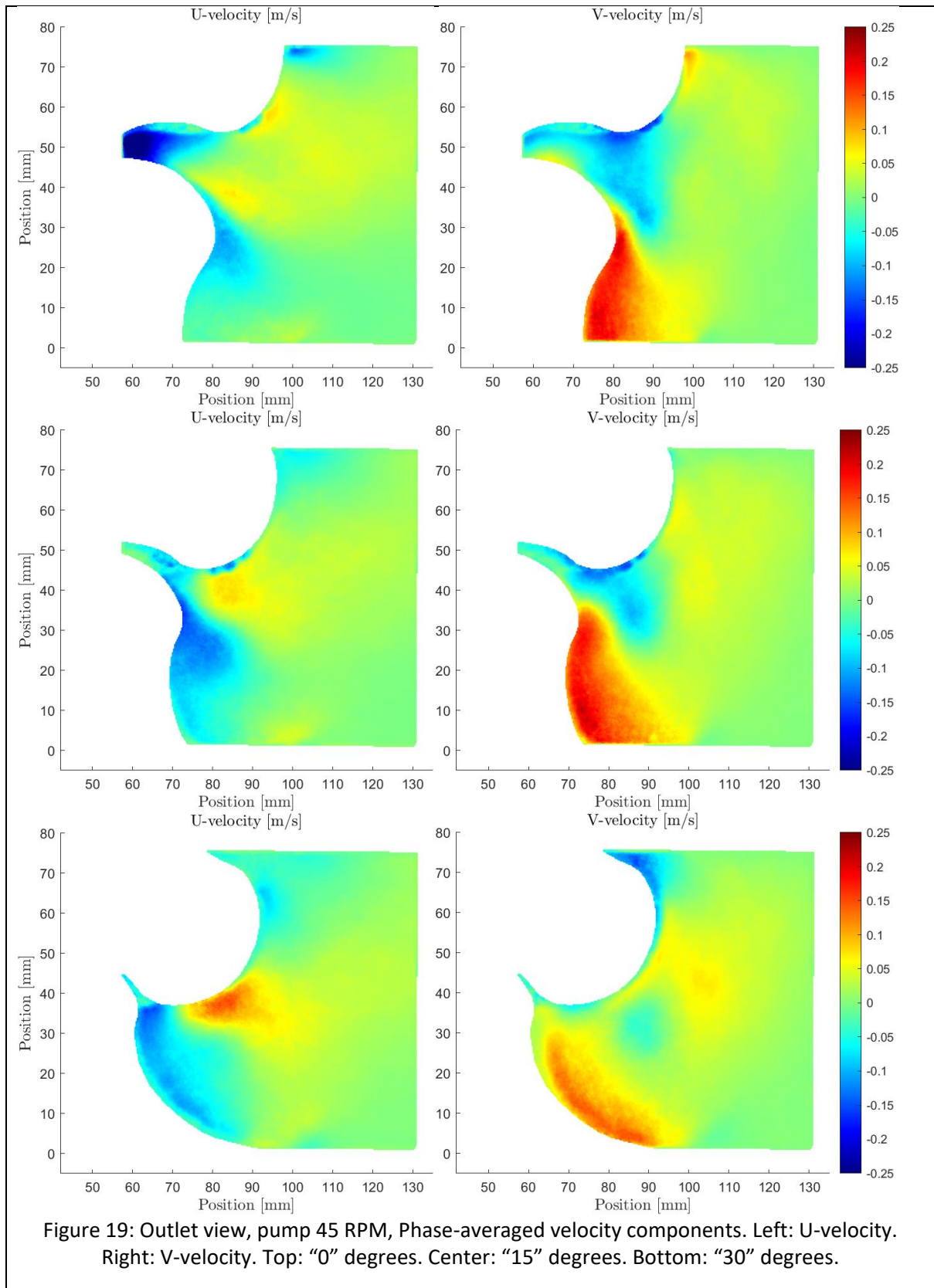


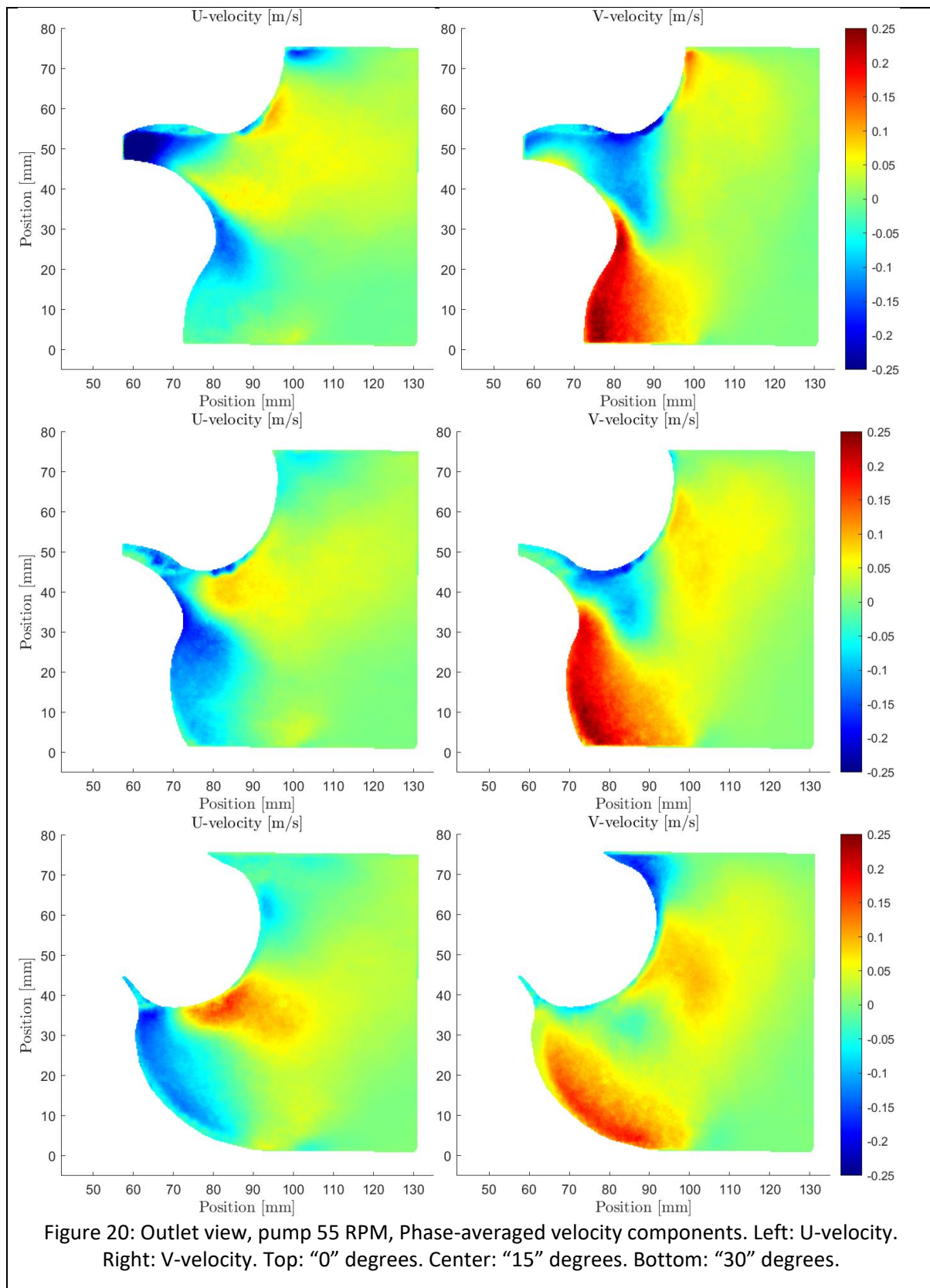


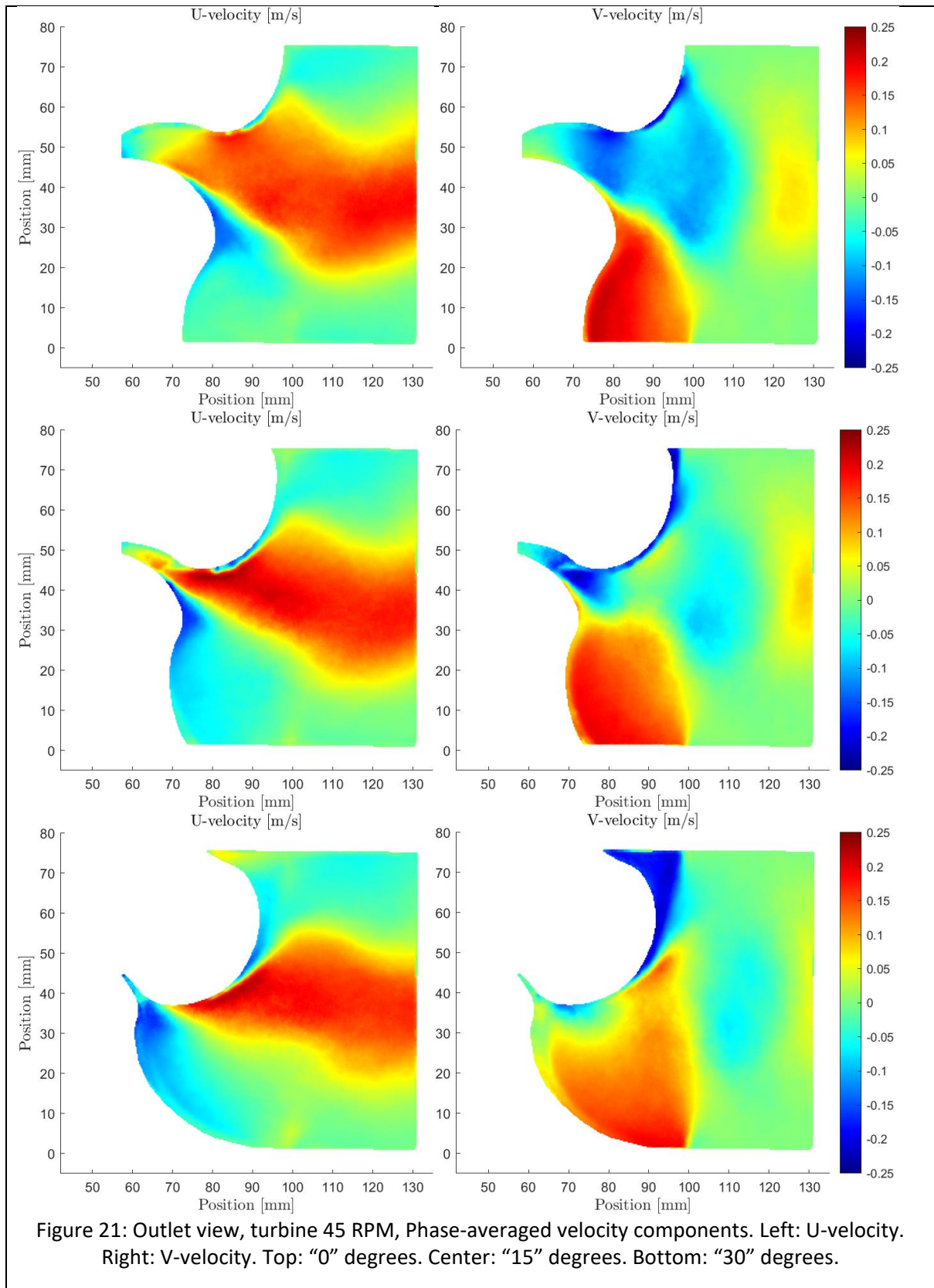












Appendix C: Contour plots of phase-averaged W velocity component at the outlet

The figures presented here show all the contour plots of the phase-averaged W velocity component for pump mode at 45 RPM, pump mode at 55 RPM, and turbine mode at 45 RPM. For each case, three phase averaging angles are shown. The W velocity component is only available from the outlet measurements with higher resolution. A positive W-component denotes a flow out of the paper. The upper and lower runner lobes in the images are rotating in the clockwise and anti-clockwise, respectively, in both turbine and pump mode. The only difference is if the pressure difference between the inlet and outlet is supporting or counteracting the flow.

It should be noted that the measured velocity component normal to the PIV plane is more *uncertain* than the components tangential to the PIV plane, although the results should give a reasonable indication of the distribution of the W velocity component.

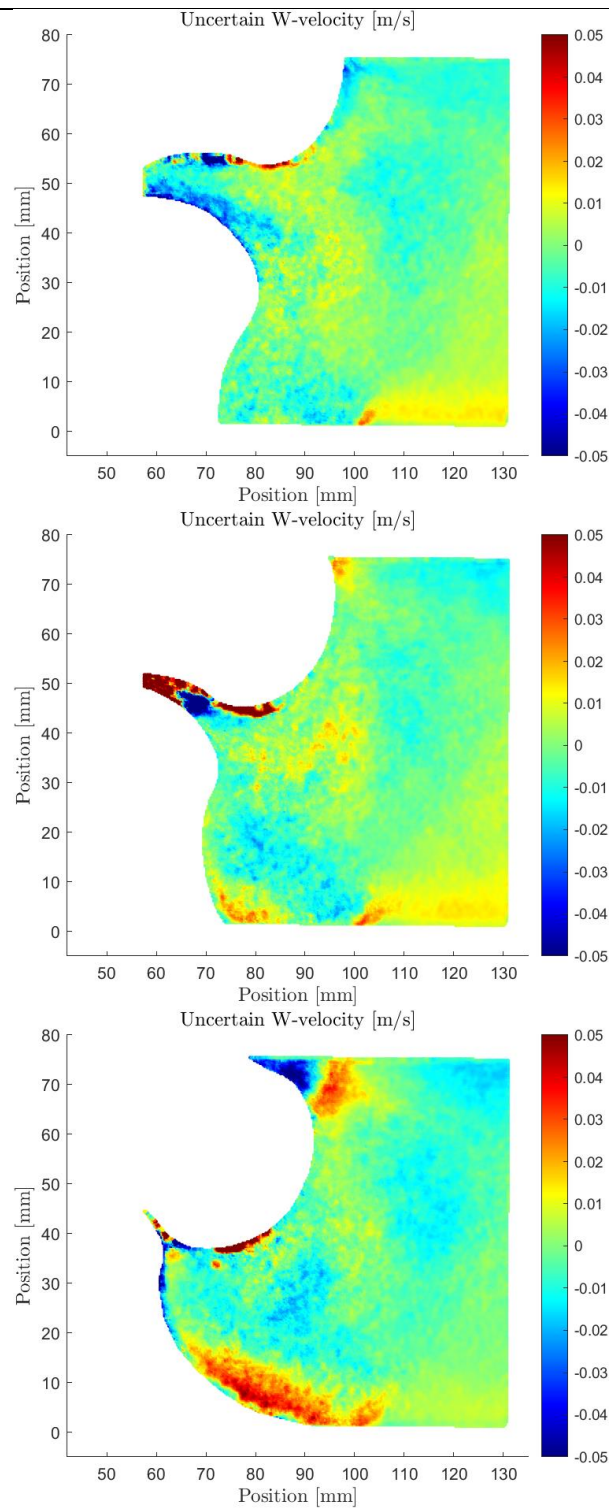


Figure 22: Outlet view, pump 45 RPM, Phase-averaged W-velocity component (uncertain).
Top: "0" degrees. Center: "15" degrees. Bottom: "30" degrees.

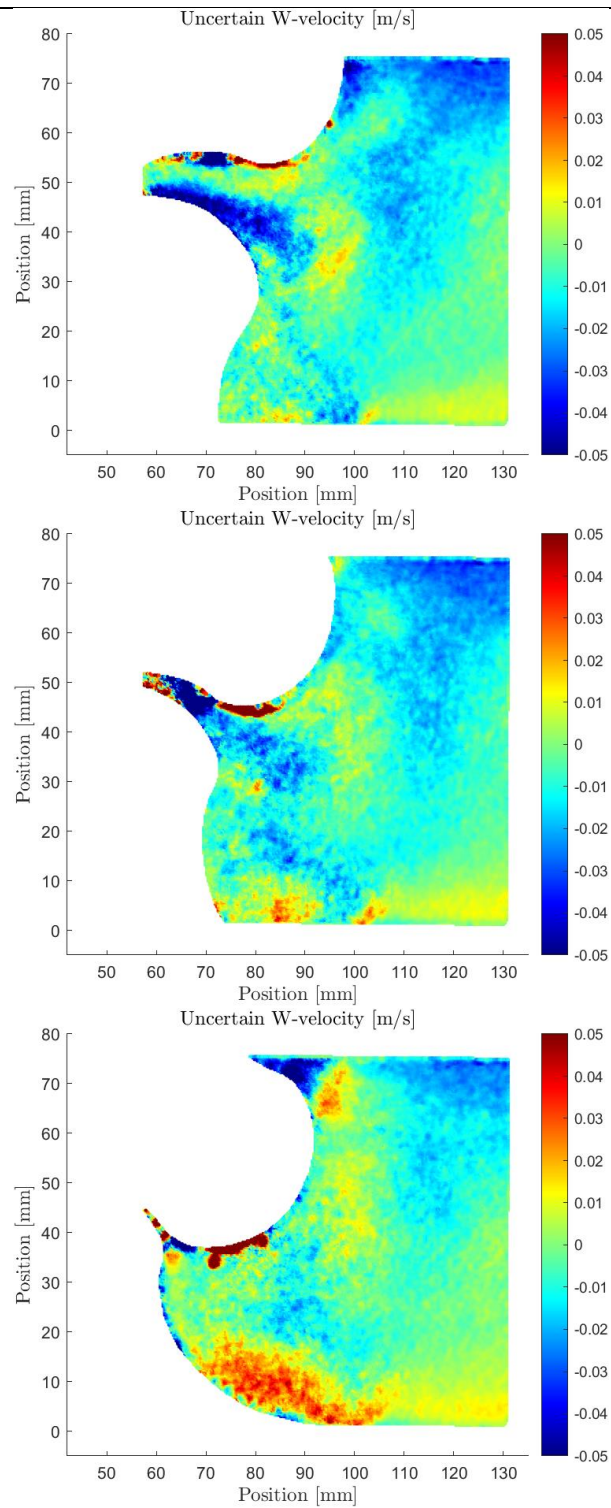


Figure 23: Outlet view, pump 55 RPM, Phase-averaged W-velocity component (uncertain).
Top: "0" degrees. Center: "15" degrees. Bottom: "30" degrees.

Appendix D: Examples of contour plots of standard deviation

The figure presented here shows examples of contour plots of standard deviation. They can be produced using the available data and post-processing scripts for all combinations shown in appendices A, B and C, but they are not all included in the report to save space.

The standard deviation is defined as

$$s = \sqrt{\frac{1}{N} \sum_{i=1}^N (x_i - \bar{x})^2},$$

where \bar{x} is the phase-averaged value and x is the instantaneous value of N samples of a particular velocity component.

The standard deviation basically gives an indication of how much an instantaneous value may differ from the average value. Thus, regions with standard deviation close to zero have rather stable velocity components at the particular phase/angle of the lobe, while regions with large standard deviation have highly varying velocity components at the particular phase/angle of the lobe.

It can be seen that the largest standard deviations typically occur in regions where the flow is influenced by the interaction between the lobes and between each lobe and the housing. In turbine-mode, it can be seen that a slightly larger standard deviation occurs in the upstream region with elevated U-velocities. This shows that that region is somewhat unstable in the phase-averaged perspective.

The upper and lower runner lobes in the images are rotating in the clockwise and anti-clockwise, respectively, in both turbine and pump mode. The only difference is if the pressure difference between the inlet and outlet is supporting or counteracting the flow.

